The Magnetohydrodynamics of Supersonic Gas Clouds: MHD Cosmic Bullets and Wind-Swept Clumps[7]

T. W. Jones[1,4], Dongsu Ryu[2,5], and I. L. Tregillis[1,3,6]

ABSTRACT

We report an extensive set of two-dimensional MHD simulations exploring the role and evolution of magnetic fields in the dynamics of supersonic plasma clumps. We examine the influence of both ambient field strength and orientation on the problem. Of those two characteristics, field orientation is far more important in the cases we have considered with $\beta_0 = p_g/p_b \geq 1$. That is due to the geometry-sensitivity of field stretching/amplification from large-scale shearing motions around the bullet. When the ambient magnetic field is transverse to the bullet motion, even a very modest field, well below equipartition strength, can be amplified by field line stretching around the bullet within a couple of bullet crushing times so that Maxwell stresses become comparable to the ram pressure associated with the bullet motion. The possibility is discussed that those situations might lead to large, induced electric potentials capable of accelerating charged particles. When the ambient field is aligned to the bullet motion, on the other hand, reconnection-prone topologies develop that shorten the stretched field and release much of the excess energy it contains. In this geometry, the Maxwell stresses on the bullet never approach the ram pressure level. In both cases, however, the presence of a field with even moderate initial strength acts to help the flow realign itself around the bullet into a smoother, more laminar form. That reduces bullet fragmentation tendencies caused by destructive instabilities. Eddies seem less effective at field amplification than flows around the bullet, because fields within eddies tend to be expelled to the eddy perimeters. Similar effects cause the magnetic field within the bullet itself to be reduced below its initial value over time.

For oblique fields, we expect that the transverse field cases modeled here are more generally relevant. What counts is whether field lines threading the face of the bullet are swept around it in a fashion that folds them (leading to reconnection) or

[1]Department of Astronomy, University of Minnesota, Minneapolis, MN 55455

[2]Department of Astronomy & Space Science, Chungnam National University, Daejeon 305-764, Korea

[3]present address: Department of Applied Physics, Cornell University, Ithaca, NY 14853

[4]e-mail: twj@astro.spa.umn.edu

[5]e-mail: ryu@sirius.chungnam.ac.kr

[6]e-mail: tregilli@msi.umn.edu

[7]Submitted to the Astrophysical Journal

that keeps them unidirectional one each side of the bullet. In the second instance, behaviors should resemble those of the transverse field cases. We estimate that this, quasi-transverse, behavior is appropriate whenever the angle, θ, between the motion and the field satisfies $tan\theta \gtrsim 1/M$, where M is the bullet Mach number.

From these simulations, we find support in either field geometry for the conclusions reached in previous studies that nonthermal radio emission associated with supersonic clumps is likely to be controlled largely by the generation of strong magnetic fields around the perimeters of the clumps, rather than local particle acceleration and field compression within the bow shock. In addition, since the magnetic pressure on the nose of the bullet likely becomes comparable to the ram pressure and hence the total pressure behind the bow shock, the gas pressure there could be substantially lower than that in a gasdynamical bullet. That means, as well, that the temperature in the region on the nose of the bullet would be lower than that predicted in the gasdynamical case. That detail could alter expectations of the thermal emission, including X-rays and UV-IR lines.

Subject headings: instabilities – ISM: supernova remnants – young stellar objects – magnetohydrodynamics: MHD

1. Introduction

In recent years observations have revealed the presence of dense, high-velocity gas clumps within and sometimes outside young supernova remnants and also associated with the outflows from young stars (*e.g.*, Braun *et al.* 1987; Allen & Burton 1993; Aschenbach *et al.* 1995; Strom *et al.* 1995). These "cosmic bullets" or, in some scenarios, "wind-swept clumps" can shine prominently in either thermal emission (*e.g.*, van den Bergh 1971; Schwartz 1975; Allen & Burton 1993; Strom *et al.* 1995) or nonthermal emission (*e.g.*, Braun *et al.* 1987; Anderson *et al.* 1994). Sometimes in supernova remnants they show elemental compositions indicating formation exclusively from material ejected out of the depths of the progenitor supernova. The exact origins of the bullets are still unclear, but suggestions range from explosive ejection (Loeb *et al.* 1995; Norman & Silk 1979) to wind-swept, pre-existing clumps (Schiano, Christiansen, & Knerr 1995), and dynamical instabilities in winds (Stone, Xu, & Mundy 1995). Whatever the manner of creation, cosmic bullets seem capable of surviving for remarkable lengths of time, thus transporting energy and mass over large distances, and have been suggested as sites for acceleration of high energy particles (*e.g.*, Coleman & Bicknell 1985; Braun *et al.* 1987; Jones, Kang, & Tregillis 1994). Yet, simple arguments and computer simulations suggest that gasdynamical instabilities may be highly disruptive of these bullets (*e.g.*, Jones, Kang, & Tregillis 1994; Schiano, Christiansen, & Knerr 1995), limiting their existence to only a few times the interval required for the applied ram pressure to crush them. That would limit their propagation distance to only a few times the length $\sqrt{\chi}R$, where χ is the density contrast with the environment and R is the bullet radius. So, only the densest clumps could survive to propagate more than a few times their own size scale.

However, in many cases one expects that both the clouds and the surrounding material are mostly ionized plasmas, so that embedded magnetic fields ought to be largely frozen in and should play a role. In a recent paper we emphasized the possibility, based on numerical simulations involving a passive magnetic field, that bullets may be effective in amplifying weak ambient magnetic fields as a side effect of the destructive interactions with their environments (Jones, Kang, & Tregillis 1994). It was emphasized there that field amplification could be more important in generation of associated nonthermal synchrotron emission, for example, than local particle acceleration in the shocks formed by the bullets (Jones & Kang 1993; Anderson *et al.* 1994; Jones, Kang, & Tregillis 1994). At the same time amplified magnetic fields could act to stabilize the Kelvin-Helmholtz and Rayleigh-Taylor instabilities, thereby limiting bullet fragmentation. That role might help account for their ability to survive, or at least for significant pieces to penetrate much farther than gasdynamical calculations suggest they might.

Mac Low *et al.* 1994 carried out two-dimensional MHD simulations of a dense plasma cloud overrun by a plane shock, demonstrating in that related case how a magnetic field might be amplified and also how it may prevent the complete destruction of the cloud in the postshock flow. Although shocked clouds and supersonic bullets are qualitatively similar objects in some ways, there are also significant differences between them, as well. In particular, as long as the impinging shock is not radiative, the material surrounding the shocked cloud is mostly moving sub-sonically

with respect to the cloud, because the cloud is overrun by a hot, postshock flow. The bullet, of course, is (by definition) interacting with a supersonic flow, at least in the beginning. This difference influences especially the flow to the rear and on the sides of the cloud and could influence instabilities and magnetic field behavior (see Jones & Kang 1993, Jones, Kang, & Tregillis 1994). Furthermore, Mac Low *et al.* 1994 considered primarily shocked clouds with a magnetic field aligned along the symmetry axis of the flow, except for one simulation involving a transverse field that was not reported in much detail. That aligned field orientation was mandated by their use of cylindrical symmetry for all but the one simulation. The other simple field geometry possible with cylindrical symmetry; namely, a toroidal one, is not a very natural one for this problem. On the other hand, the geometry of the magnetic field ought to be very important to its evolution in and around the dense cloud and also to its dynamical influence on the cloud. We may also expect the influence of the magnetic field to depend on its strength. These issues in the bullet context have not been addressed before in the literature.

In this study we present results from two-dimensional, full MHD simulations of the evolution of dense supersonic plasma bullets with magnetic field geometries both aligned with the bullet motion and also transverse to it. In order to have freedom in the field geometry, the simulations have been done in Cartesian coordinates rather than in cylindrical coordinates. Also we have simulated flows using a range of magnetic field strengths and using a range of numerical resolutions. One can envision the bullets either as ejecta or as condensations being swept by a supersonic wind. Our objectives are to understand better how the field in and around the bullet is influenced by the bullet and also how the magnetic field acts on the bullet dynamically. §2 outlines the important dynamical issues, while §3 describes the numerical methods we employ. In §4 we describe our results, while a brief summary of the principal conclusions is presented in §5.

2. The Dynamical Problem

The basic issues associated with the interaction between a gas bullet and its surroundings are well-known, so readers are referred to the extant literature for detailed discussions (*e.g.*, Jones, Kang, & Tregillis 1994; Schiano, Christiansen, & Knerr 1995 and references therein) or for comparisons with shocked clouds (*e.g.*, Jones & Kang 1993; Klein *et al.* 1994; Mac Low *et al.* 1994; Xu & Stone 1995). In this section we present only a brief outline of the issues to facilitate later evaluation of the particular new issues raised in this study.

2.1. Problem Definition

As in previous studies we consider the bullet to be initially in pressure equilibrium with the ambient medium and the initial magnetic field to be uniform through both the bullet and the ambient medium. The plasma is assumed throughout to be highly conducting, so that magnetic

field is frozen in. At $t = 0$ the bullet is set into motion at speed u_{b0} with respect to the ambient medium. If such complications as radiative cooling, thermal conduction, and gravity can be neglected, the bullet dynamics is determined by a minimum of the following six parameters and the bullet shape: the sonic Mach number of the bullet through the ambient medium, $M = u_{b0}/c_{sa}$; the gas adiabatic index, γ; the density contrast between the bullet and the ambient background, $\chi = \rho_b/\rho_a$; as well as the magnetic field strength, B_0, and orientation (generally, two angles). The initial strength of the magnetic field can be expressed either in terms of the Alfvénic Mach number $M_A = u_{b0}/a$, where a is the Alfvén speed, or in terms of $\beta_0 = p_g/p_b = (2/\gamma)(M_A/M)^2$. The field orientation can be specified by the angle, θ, between the field, B_0, and the bullet velocity, u_{b0}, as well as between B_0 and any distinct symmetry axis or plane for the bullet.

Fortunately, as previous shocked-cloud studies emphasized (Klein *et al.* 1994; Mac Low *et al.* 1994), in the limit $M >> 1$, the sonic Mach number can be scaled out of the problem. Xu & Stone 1995 found in three-dimensional gasdynamical simulations of shocked clouds that the initial morphology of the cloud does make a quantitative difference in its evolution, but that qualitative features are not very geometry-sensitive. Thus, we will consider only a single initial Mach number and a single bullet morphology. Because three-dimensional MHD simulations of sufficient numerical resolution are still too expensive to follow magnetic fields adequately in this problem, we have used two-dimensional symmetry. We are concerned, on the other hand, with influences of different magnetic field geometries with respect to the bullet and its motion, so we have chosen a Cartesian coordinate system, which enables us to set up a uniform magnetic field with arbitrary orientation. In this geometry the simplest initial cloud morphology is a circular cylinder, with its axis out of the computational plane and thus orthogonal to the motion of the bullet. Although we have actually carried out test simulations in which the magnetic field has a component out of the plane (and, thus, aligned with the bullet axis), we present here only cases for which the magnetic field is entirely in the computational plane and either aligned to the direction of the bullet motion or transverse to it. We have found no qualitatively different behaviors for the fields with a component out of the plane.

The characteristic evolutionary timescale of a bullet is the so-called "bullet crushing time",

$$t_{bc} = \frac{2R\sqrt{\chi}}{u_{b0}}, \tag{1}$$

where R is the initial bullet radius. It allows one to subsume the values of the initial density ratio, χ, and speed, u_{b0}, into one parameter. It is traditional in studies such as this to consider a single, convenient value for each of these, and to discuss the evolution as though it depended only on t/t_{bc} and not on χ, for example. We will follow this procedure, but also comment on its limits. In addition we set $\gamma = 5/3$. We are left, then, with a two-dimensional parameter space to explore; namely, we need to define the strength and the orientation of the magnetic field relative to the bullet motion in the plane.

2.2. Issues

Once set in motion, the bullet history begins through formation of a shock pair; namely, a strong bow shock that surrounds the bullet and an equally strong, internal or "bullet shock", that propagates through the bullet from nose to tail compressing it along the direction of motion. The time, t_{bc}, defined in Eq. 1 measures the interval required for the ram-pressure-driven bullet shock to cross the bullet diameter. Note that our definition for t_{bc} contains an additional factor of two compared to that normally used in discussions of shocked clouds. Before t_{bc}, the bow shock is established and flows along the bullet boundary may lead to some stripping due to small-scale Kelvin-Helmholtz (K-H) instabilities. On a timescale comparable to or exceeding t_{bc}, both K-H and Rayleigh-Taylor (R-T) instabilities with scales comparable to the size of the bullet can begin to develop. Gasdynamical calculations mentioned earlier show R-T instability-induced bubbles with low density, ambient plasma penetrating through the bullet body, beginning a fragmentation process. K-H instabilities along boundaries allow small pieces of the bullet to be stripped, so eventually one expects the gas bullet to be broken into a "mist" and then dispersed. Estimates for this "dispersal" time are consistent for both bullet and shocked cloud simulations. Although the dispersal timescale is difficult to define uniquely, all gasdynamical simulations show significant signs of bullet disruption by about $t \sim 2 - 3t_{bc}$ (using our definition for the time unit). Before the bullet is fully disrupted, ram pressure decelerates it substantially (or if it is seen as a wind-swept clump, accelerates it in the direction of the wind). That deceleration, of course, is the origin of the R-T instability. The deceleration is considerably enhanced by lateral expansion of the bullet coming from the penetration of the bubbles induced by R-T instabilities.

The simulations presented by Jones, Kang, & Tregillis 1994 and Mac Low *et al.* 1994 showed that weak magnetic fields in the ambient medium can be stretched and thus strengthened through sheared gas motions around clouds. Compression can also increase field strength, but that process is generally much less significant in complex flows than stretching. Mac Low *et al.* 1994 concluded from their shocked cloud simulations that the fields can sometimes be amplified until $p_b \sim \rho_a u_b^2$. Field enhancement through stretching takes place in three situations. Mac Low *et al.* 1994 emphasized the importance in their axial geometry of field lines aligned along the symmetry axis being stretched along the symmetry-axis, behind their shocked cloud, while a Mach disk carries away (conducting) material from the cloud as it catches up to the originally incident shock in recession. Jones, Kang, & Tregillis 1994 emphasized in their transverse field geometry the importance of field lines being stretched around the cloud perimeter as they envelope the cloud. In addition, for either field geometry, vortices that form, especially in the immediate wake of the cloud, could stretch entrained field lines and, thus, amplify them. Field amplification within vortices is complex, however, because it involves field lines that are wrapped around until they are adjacent to fields of opposite direction. That is unstable to reconnection, so that within the vortices field line reconnection will limit the field growth and effectively expel magnetic flux (*e.g.*, Weiss 1966; Galloway & Weiss 1981) to the vortex perimeter. For numerical simulations of ideal MHD, the resistivity that allows reconnection to take place comes from numerical truncation and

the associated dissipation, so it is locally resolution dependent. That means one needs to be cautious in understanding the convergence properties of fields. We emphasize, however, that with the fully conservative methods we employ (including mass, momentum, total energy and magnetic flux), the reconnective process is a necessary consequence, not an added feature.

Mac Low *et al.* 1994 found from their shocked cloud simulations that inclusion of a dynamical magnetic field did significantly enhance the durability of their clouds, and concluded that this was primarily due to the influence of the magnetic field in inhibiting the vortices that form along the slip surfaces on the sides and rear of the cloud. Although Mac Low *et al.* 1994 defined their initial field strength so that $\beta_0 = 1$ for most of the runs they did, this was based on the *preshock* ambient plasma. Behind the incident (Mach 10) shock, where the interactions are taking place, $\beta_0 \propto M^2 >> 1$. Thus, the field interacting with the clouds is initially relatively weak. A similar consideration applies to the MHD bullet problem, especially in the cases with the field aligned to the bullet motion, since the value of β behind the bow shock of the bullet is also increased by a factor $\sim M^2$.

3. Numerical Method & Setup

Our simulations have been carried out using a code for compressible, ideal MHD based on a conservative, explicit TVD method as described in Ryu & Jones 1995 and Ryu, Jones, & Frank 1995. The scheme, utilizing an approximate MHD Riemann solver, is second order accurate in both space and time and cleanly captures all the various families of MHD discontinuities. We have used the multidimensional, Cartesian version of the code that was previously applied successfully to the study of the nonlinear MHD K-H instability in modestly compressible conditions (Frank *et al.* 1996), a problem that demonstrates the code's ability to follow accurately smooth but complex MHD flows. The code maintains $\nabla \cdot B = 0$ to machine accuracy by employing a simple, corrective transformation at each time step (Brackwell & Barnes 1980) utilizing an exact Fourier transform relationship as a key feature to maintain both accuracy and speed in this step (Ryu, Jones, & Frank 1995). The simulations are two and a half $(2 + 1/2)$ dimensional; *i.e.*, vector fields include three components, but all fields are independent of the z-coordinate. The results presented all involve flows with $B_z = u_z = 0$, however.

In each presented computation the bullet is placed with its diameter along the x-axis, and reflection symmetry assumed across that axis, so that only the upper half of the flow structure has been computed. We have carried out several comparison test simulations, however, using the full flow to demonstrate an exact correspondence with the more economical computations presented. The top and right boundaries of the grid are open, while the left boundary is "flow-in" to maintain the upstream wind conditions exactly.

The bullet initially has a circular cross section with a radius $R = 50/51.2 = 0.97656$. This, slightly noninteger value resulted from our definitions of the bullet radius in zones (*e.g.*50) that

did not quite match onto the grid sizes that we used (*e.g.*512). Inside this radius the bullet density is $\rho_b = \chi\rho_a$ with $\rho_a = 1$. A thin boundary layer with a hyperbolic tangent profile has been applied to the bullet, using a characteristic width of two zones. Since the grid is Cartesian, the bullet has a cylindrical form and its axis is aligned with the z-direction. The computational domain is $x = [0, 10]$, $y = [0, 5]$. At the start of each computation the bullet center is $(x_c, y_c) = (1.5, 0)$. Each simulation begins with the bullet at rest while an ambient medium flows from left to right at speed $u_{b0} = 10 = M$, so that the sound speed in the ambient medium, $c_{sa} = \sqrt{\gamma p_0/\rho_a}$, is unity. Interaction with this "wind" accelerates the bullet towards the positive x-direction. In a fixed frame this would cause the bullet to be expelled from the grid on a timescale of only $\sim 2t_{bc}$. In order to enable the simulations to follow the bullet evolution as long as possible, we have incorporated a feature that adjusts the reference frame speed at each time step so that the intersection of the bullet bow shock with the x-axis is approximately stationary on the grid. The bullet still moves slowly towards the right grid boundary as the Mach number of the bow shock decreases and the stand-off distance between the shock and the bullet nose increases. But this procedure has enabled us to follow bullet evolution for at least 4 t_{bc} and more typically 8 t_{bc}.

We have used a range of numerical resolutions. Following Klein *et al.* 1994, we have characterized them in terms of the number of zones across one bullet radius; *e.g.*, R_{50}, refers to a simulation with 50 zones across the bullet radius. Since the grid is uniform the total number of zones would be 512×256 for an R_{50} run and 1024×512 for an R_{100} run, for examples.

To understand better the evolution of the bullet, we have included a passive, Lagrangian, conserved "tracer", f, that can be termed the "bullet fraction" or, in the language of Xu & Stone 1995, the "color" of the fluid. This is set equal to unity for fluid initially inside the bullet ($f = 1$) and zero ($f = 0$) everywhere else. The bullet fraction is followed with a TVD advection routine identical to that utilized for mass advection in the code. This enables us to compute several useful quantities, such as the bullet mass inside the grid,

$$M_{bull} = \int_V f\rho dV, \tag{2}$$

where $dV = dxdy$ and V represents the volume of the entire calculation domain. Other related useful quantities include the mass-weighted speed of the bullet,

$$\bar{u}_b = \frac{1}{M_{bull}} \int_V u_x f\rho dV, \tag{3}$$

and the mean height of the bullet in the y-direction,

$$\bar{h}_{bul} = \frac{1}{M_{bull}} \int_V yf\rho dV. \tag{4}$$

We will present $\bar{u}_b$ as measured in the initial rest frame of the bullet. At the start $\bar{h}_{bul} = 4R/3\pi = 0.414$. Another useful integrated quantity is the magnetic energy enhancement inside the grid. That is conveniently normalized in terms of the magnetic energy initially inside

the bullet, $E_{Bob} = (3/5)(\pi R^2/2\beta_0)$, where we set $c_{sa} = \rho_a = 1$, and $\gamma = 5/3$. Then using the initial total magnetic energy inside the computational domain, $E_{Bo} = (3/5)(5 \times 10/\beta_0)$, we have

$$\Delta E_{mag} = \frac{1}{E_{Bob}}\left[\int_V \frac{1}{2}(B_x^2 \ + \ B_y^2)dV - E_{Bo}\right], \tag{5}$$

where $p_b = \frac{1}{2}B^2$ in our units.

4. Results

As mentioned earlier we have carried out simulations with two initial magnetic field geometries; namely a field transverse to the motion of the bullet (henceforth identified as "T" models) and parallel or aligned with the bullet motion (henceforth identified as "A" models). Table 1 characterizes six MHD simulation pairs with a range of field strengths for each geometry. Models T1–T5 and A1–A5 include 50 zones across a radius (thus, termed R_{50} runs) while T6 and A6 use 100 zones (R_{100} runs). Three additional, control models, N1–N3, have set the magnetic field to zero. They vary χ, but are otherwise identical to the T1–T5 and A1–A5 models. These purely gasdynamical cases are intended to assist in identifying MHD effects on the flows that might develop even when the field is initially weak. In addition we have explored the degree to which flow behaviors depend on the density contrast, χ, enabling us to compare the current simulations with our previous ones. All of the MHD models have assumed $\chi = 10$, while the gasdynamical models, N1,N2 and N3 have used $\chi = 10$, 40 and 100, respectively. The duration of each run is indicated in Table 1 as t_{end}.

The appendix evaluates "convergence" issues associated with the grid. To summarize quickly the appended discussion, we conclude that the R_{50} simulations are well converged by such global measures as the quantities defined in Eqs. 2–4. The magnetic energy enhancement (Eq. 5) is reasonably well converged in the transverse field cases and in the aligned field cases at early times. However, the topology of the aligned field makes it more sensitive to the details of eddy structures that form around the bullet as it is destroyed, and those details depend on numerical resolution. So, at late times the magnetic energy enhancement is not converged in our aligned-field simulations. In association with this, it is clear that structural details of the bullets at late times, $t/t_{bc} >> 1$, do depend on resolution, especially since the perturbations in the bullet structure that eventually lead to its destruction come out of the mismatch between the bullet geometry and the grid geometry in our simulations. Those aspects should serve as reminders that calculations such as these are idealized efforts to understand the physics of clouds interacting with their environments and not intended to be used as predictors of detailed structures. That point is also made stronger by the recognition that bullet evolution, particularly after $t/t_{bc} = 1$, depends physically on the initial bullet structure, including the bullet geometry (see Xu & Stone 1995) and the density contrast (see discussion below).

Figs. 1, 2 and 3 contain images that provide a summary spanning pretty well the behaviors

of the MHD models we have computed before significant mass stripped from the bullets begins to leave the grid. Panels (a) and (b) in each of those figures represent transverse field cases, with T2 ($\beta_0 = 4$) in (a) and T5 ($\beta_0 = 256$) in (b). Panels (c) and (d) represent the analogous aligned field cases, with A2 in (c) and A5 in (d). For each model two times are shown: $t/t_{bc} = 2$ and 6. Fig. 1 illustrates evolutionary aspects of the log gas density, Fig. 2 shows the magnetic field lines and Fig. 3 the vorticity. In the appendix, Figs. a1 and a2 show log density and field lines at $t/t_{bc} = 4/3$ and 4 for models T5 and A5 as well as their higher resolution representations, T6 and A6. For comparison, Fig. 4 illustrates the log density distributions for the gasdynamical models N1–N3 at $t/t_{bc} = 1$ and 2.

4.1. Bullet Evolution: Aligned Field Cases

It is convenient to begin our discussion with an outline of the evolution of bullet structures and associated magnetic fields in the cases with fields aligned to the direction of the bullet motion. Those show less dramatic dynamical differences from the gasdynamical bullets discussed in Jones, Kang, & Tregillis 1994, and closely resemble in some ways the aligned field simulations of shocked MHD clouds described in Mac Low *et al.* 1994. Several key points are clear from the figures listed above. First, in all the aligned-field cases the bullet shows signs of penetration by one or more large R-T bubbles by $t/t_{bc} = 2$. There is little effect from the magnetic field on the bullet structure by this time. That impression extends to the strongest field cases we considered; namely, A2 ($\beta_0 = 4$) and A1 ($\beta_0 = 1$). Indeed, the density distributions for A2 and A5 at this time are very similar and also hardly distinguishable from the analogous run with $B = 0$, model N1 (see Figs. 1 and 4). This comparison is more quantitatively apparent in Fig. 5, which includes plots of density, ρ, velocity as measured in the initial rest frame of the bullet, u_x, gas pressure, p_g, and magnetic pressure, p_b, along a cut just above the x-axis for the same situations as in Figs. 1, 2, and 3. The solid lines correspond to $t/t_{bc} = 2$, while dotted lines illustrate quantities at $t/t_{bc} = 6$. Furthermore, the vorticity structure around the bullet is practically the same for both A2 and A5 (Fig. 3) providing a very good indicator that the dynamics in the two models are very similar at this time (see, *e.g.*, Klein *et al.* 1994). Qualitatively this vorticity structure is also the same as that found in three-dimensional gasdynamical simulations of shocked clouds at comparable dynamical times (Xu & Stone 1995). The vorticity associated with flow over the bullet is negative (clockwise). We see in Fig. 3 that in the stronger field case, A2, some vorticity of the opposite sign has been generated in the bullet wake in response to magnetic tension there, however.

Comparing at $t/t_{bc} = 2$ model A5 in Fig. 1 with model N1 shown in Fig. 4, we see no detectable difference in density distributions. The field has not had any appreciable influence on the development of R-T and K-H instabilities, since it is not strong enough anywhere along the bullet boundary to suppress them directly. K-H instabilities will be suppressed by the field along the boundary according to linear theory, if the local Alfvén speed exceeds roughly the velocity difference across the boundary (Chandrasekhar 1961). Since the local Mach number of the flow

along the bullet boundary is generally less than or about unity, the criterion for the magnetic field removing K-H instabilities is roughly $\beta \lesssim 1$ along the bullet boundary. Similarly if the Alfvén wave crossing time through a bubble perturbation on the bullet edge is less than the "buoyancy rise time", $1/\sqrt{a\lambda}$ where a is the acceleration and λ is the length scale, the magnetic field will inhibit R-T instabilities. Using Eq. 7 (see below) to estimate the acceleration of the bullet, we obtain a rough criterion for the magnetic field to stabilize R-T instabilities; namely, $\beta \lesssim \chi/M$. That leads in the present context again to $\beta \lesssim 1$, since $\chi = M$. Even in the case A1 with $\beta_0 = 1$, the local β along the bullet face and sides is everywhere greater than unity. In fact, we do not find at any time in aligned field models A1–A6 that the magnetic field adjacent to the bullet is ever strong enough that $\beta \leq 1$ (there is one region with $\beta << 1$ in the wake, as we will discuss below). However, even a relatively weak magnetic field can play a significant role in small scale flow dynamics, as pointed out by others (*e.g.*, Cattaneo & Vainstein 1991; Frank *et al.* 1996) and as we shall explain further on.

By $t/t_{bc} = 2$ the states of K-H and R-T instabilities are, on the other hand, rather strongly influenced by the density contrast choice, $\chi = 10$. The other panels in Fig. 4 illustrate how, as the density contrast is increased, the penetration of the R-T bubbles into the bullet is enhanced for fixed t/t_{bc}. While, in the limit of large χ, the linear growth times on a given length for both K-H and R-T instabilities scale directly with t_{bc}, both growth rates include an additional term that increases with χ when it is finite. That tendency is consistent with the behaviors illustrated in Fig. 4. As a further test, we can compare run N3 ($\chi = 100$) with very similar gasdynamic simulations reported in Jones, Kang, & Tregillis 1994. Those earlier simulations were carried out using a PPM gasdynamic code and were designed to study dynamical feedback on bullets from cosmic-rays accelerated in shocks associated with the bullet. However, model number 1 in that paper omitted cosmic-rays. Their Fig. 4 illustrates density structure at $t/t_{bc} = 2$, showing a good correspondence between the cloud structures in the two simulations, except that our current calculations show less evidence of small scale K-H structures along the bullet boundary. Even when $B = 0$ the MHD TVD code does suppress the smallest scale K-H instabilities in comparison with the PPM code, because it spreads the very strong contact shear layer of the bullet edge over several more zones. K-H instabilities are suppressed on scales less than the thickness of the shear layer.

As a direct consequence of the penetration of the R-T bubbles, the bullet begins appreciably to expand laterally by $t/t_{bc} \sim 2$. For all the aligned field cases, the mass weighted bullet height, $\bar{h}_{bul}$, has expanded to roughly five times or more its initial value by $t/t_{bc} = 6$ (see Fig. 6). This characteristic behavior was also noted by others with regard to gasdynamic simulations. As illustrated in Fig. a1, before $t/t_{bc} = 4$, our bullets develop a roughly "C"-shaped morphology on the computed half-plane in all of the aligned field cases, A1-A5. (Including the reflected portion below the computed space, the cloud shape would be an "E".)[8] That "C" continues to open up and thin itself even until the bullet moves off the grid. As the figures show bullet mass is stripped

and carried into the wake, eroding the bullet body.

In response to drag forces the bullet is accelerated towards a terminal velocity, u_{b0}, as measured in the original reference frame; that is, the bullet or its fragments should come to rest in the surrounding flow. Klein *et al.* 1994 derived a simple theoretical model for the acceleration of a cloud based on ram pressure, taking into account the lateral expansion. The drag force actually comes from the difference in the total pressure across the bullet. Assuming highly supersonic motion, we can estimate in the gasdynamic case from Bernoulli's equation the pressure difference on the symmetry axis to be $\Delta p \approx (4/5)\rho_a(u_x - u_{b0})^2$, where $u_x(t)$ is the instantaneous speed of the bullet with respect to its initial reference frame and we have set $\gamma = 5/3$. Applied across the full bullet this leads to the usual expression for its acceleration,

$$\frac{d\bar{u}_b}{dt} = \frac{3}{4}\frac{C_d}{t_{bc}}\frac{(u_x - u_{b0})^2}{\sqrt{\chi}u_{b0}}\frac{r^2(t)}{R^2}, \tag{6}$$

where C_d is a drag coefficient that absorbs our ignorance of details of the pressure distribution and $r(t)$ is the effective bullet radius as a function of time. Borrowing the notion in Klein *et al.* 1994 that the bullet expansion begins only after $t/t_{bc} = 1$, we write $r^2(t) \sim R^2[1 + C_e(t/t_{bc})^2]$ where we can term C_e an expansion coefficient (see also Zahnle 1992, Mac Low & Zahnle 1994). If $C_e > 0$, drag on the bullet increases with time, enhancing its acceleration. In an MHD flow we have to account for magnetic pressure in Eq. 6. For aligned cases, however, the magnetic pressure does not enter into the Bernoulli equation on axis and the magnetic pressure is not significant anyway. Thus we expect the bullet motion to behave pretty much as in the gasdynamic case. We will comment later on modifications to Eq. 6 appropriate to transverse field cases. Eq. 6 can be integrated to give

$$\bar{u}_b = u_{b0}\left(1 - \frac{1}{1 + \frac{3}{4}\frac{C_d}{\sqrt{\chi}}\left(\frac{t}{t_{bc}}\right)\left[1 + C_e\left(\frac{t}{t_{bc}}\right)^2\right]}\right). \tag{7}$$

All the aligned field cases can be fit well with a drag coefficient, $C_d \approx 1$, and an expansion coefficient, $C_e \approx 0.05$. There is a weak trend visible in Fig. 6 for the acceleration of the bullets to be faster when the field is smaller, corresponding to a value of C_e that depends inversely on β_0. That just reflects the fact that stronger aligned fields do resist lateral expansion, keeping the bullet cross section somewhat smaller.

We expect the magnetic fields themselves to respond differently to the motion of the bullet for the two field geometries we have used. That is apparent even by $t/t_{bc} = 1$ as shown in Fig. a2. The evolution of the aligned field is similar to that found by Mac Low *et al.* 1994 for shocked

[8] As indicated earlier, the specifics of bullet morphology depend on a number of details, both physical and numerical. So the "C" shape more generally represents the fact that some number of dense R-T fingers will protrude in a forward direction, while light R-T bubbles will push into and expand the bullet body.

clouds with aligned fields. To the front of the bullet, field lines that initially pass through the bullet are swept and then "folded" over the top of the bullet in a configuration that is unstable to the resistive tearing mode. That instability leads to "magnetic islands" within and behind the bullet as seen at $t/t_{bc} = 1$ in Fig. a2 c and d or at $t/t_{bc} = 2$ in Fig. 2 c and d. The compact magnetic island closest to the axis coincides with the strong vortex at the rear of the bullet (Fig. 3). Magnetic flux initially formed into these islands is mostly annihilated by about $t/t_{bc} = 4$ (or more properly "expelled", since the total magnetic flux through the computational box does not change over time for the aligned field configuration). Magnetic reconnection also takes place inside the bullet in consequence of the circulation developing after the bullet shock has exited (see Figs. 2, 3, and a2). That significantly reduces the field strength within the bullet over time. Through these reconnection events, magnetic flux is separated into two elements: that which passes around the bullet without reversal and that which passes through the bullet. The latter flux element continues to be involved with vortices around the bullet and subjected to reversals and reconnection.

Before the magnetic flux separation, there is a thin region of strongly concentrated field formed along the axis behind the bullet, analogous to the "flux rope" discussed for shocked clouds in some detail by Mac Low *et al.* 1994. In our situation, as in theirs, this feature forms as a consequence of compression of field into the low pressure wake behind the bullet, followed by field-line stretching. In our case those field lines are temporarily anchored in the bullet on one end and drawn out to the rear by the expanding rarefaction wave (see Figs. a1 and a2). Just as for the shocked cloud case considered by Mac Low *et al.* 1994, the magnetic field in this region can become locally dominant with $\beta \leq 10^{-1}$. However, as Fig. 2 shows clearly, the field configuration on the edge of the flux rope is susceptible to tearing mode instabilities, so that the rear flux rope disappears as part of the flux separation event. We do *not* see in any of our aligned field simulations that $p_b \sim \rho_a u_b^2$, nor that this flux rope plays a significant dynamical role in the evolution of the bullet. However, this feature is the dominant source of enhanced magnetic field energy before its flux is expelled (see Fig. 6). The normalized magnetic energy enhancement, ΔE_{mag}, (Eq. 5) peaks at values between 10 and 100 near $t/t_{bc} \sim 1.5$ (see Fig. 6). The peak value in model A1 ($\beta_0 = 1$, $\Delta E_{mag} = 18$) is about half that reported by Mac Low *et al.* 1994 for their shocked cloud during this phase for the same numerical resolution across the cloud and the same β_0. Since our post-bullet flux rope is significantly thinner than theirs, the comparison seems very good. Our higher resolution, R_{100}, weak field run, A6, differs in ΔE_{mag} by $\lesssim$20% from the analogous low resolution, R_{50}, A5 run for $t/t_{bc} < 4$. So, through this stage the magnetic energy behavior seems well converged.

For the aligned field geometry there is very little compression of the field, so from the start we should expect that field line stretching would be the primary contributor to magnetic field enhancement. Along the boundary of the bullet the field remains weak before about $t/t_{bc} = 4$, even in the $\beta_0 = 1$ case, because it is subject to reconnection that shortens the field lines. However, that reconnection leads directly to the flux separation mentioned, and through that the field topology

above the bullet returns to something resembling its initial form; namely, field lines pass directly around the bullet from front to back without folding. As the bullet body expands laterally, lines above it are stretched significantly (see Fig. 2), but are no longer subject to reconnection.

A relatively thin flux tube especially on the rear perimeter of the bullet envelops the now-distended cloud, extending into the wake. Almost independently of the initial β_0 or the numerical resolution, the minimum local β is ~ 10 in this structure. After the flux separation event these field lines do not penetrate the strong vortex at the rear of the bullet. On the other hand, the flux that now passes through the bullet is drawn into the big R-T bubble and an associated vortex pair. Through reconnection, however, those field lines divide into magnetic islands (for the weaker initial field cases) that are annihilated and flux that penetrates directly through the bullet. Some flux passing through the bullet is drawn into the strong vortex at the rear and base of the bullet, leading to another region of strong magnetic flux on its perimeter. Even though the magnetic pressure in these flux tubes is never dominant, the field can still play a major role in reducing the vorticity and leading the flow to become more nearly laminar and less disruptive. That dynamical behavior was shown recently in high resolution simulations of the MHD K-H instability (Frank *et al.* 1996). There it was found in K-H unstable MHD flows that even when $\beta \gtrsim 30$ the magnetic field, acting as catalyst, realigns the flow into a stable, broad and laminar shear layer. The field acts as a catalyst in the sense that kinetic energy is temporarily stored in the field so that locally the magnetic tension is at least significant if not dominant. That stored energy is released again during reconnection, but one result of the reconnection is that the velocity and magnetic fields are more closely aligned; that is, the magnitude of the cross helicity is increased. The smoothing and spreading of the flow should significantly reduce stripping from the bullet. This conclusion is consistent with that reached by Mac Low *et al.* 1994, that the magnetic field reduces the intensity of vortices around their clouds and, thus, increases the cloud survivability. The presence of the magnetic field is clearly felt by the bullets in our aligned field simulations. Clouds in the stronger field cases are less distended (Figs. 1, 2, and 6) and there is an apparently stable density concentration at the top of the bullet "C". Examination of the forces applied there shows that the density is mostly confined by ram pressure, but that magnetic pressure and tension contribute at the 10% level, as anticipated from earlier discussion. At late times in these cases material no longer seems to be stripped from the bullets (see Fig. 6), consistent with our comments above. For the stronger field cases, there is less thinning of the main bullet body, as well.

Magnetic energy enhancement in the aligned field models begins to rise again after $t/t_{bc} \sim 4$, mostly in response to the development of flux tubes around the bullet and in the associated vortices. Our simulations are not able to capture this final rise completely, because the flux tube fine structures are still resolution dependent (see Figs. a2 and a4) and because significant magnetic structures begin to leave the grid after $t/t_{bc} \sim 7$. It appears likely, however, that the excess magnetic energy becomes at least comparable in this stage to the peak value noted earlier. Mac Low *et al.* 1994 similarly emphasized the lack of convergence in the magnetic field within their

simulations. They also used an aligned field geometry, so the issues responsible were analogous.

Although the details are fairly complex, the summary of aligned-field bullet evolution is straightforward. Magnetic fields are initially swept over the bullet, stretched and folded there. Eventually reconnection separates the field into flux passing directly through the bullet and flux passing directly around it. Except within a thin flux tube formed temporarily along the symmetry axis, there is no place that the magnetic field becomes energetically dominant; that is, almost everywhere $\beta >> 1$. In the meantime the disruptive, ram pressure force that applies to gasdynamical bullets (and gasdynamical shocked clouds) causes the initial cloud to become distended and stripped. Magnetic field stretched over the top of the bullet can have a significant stabilizing influence that should prolong bullet coherence even though magnetic energy never becomes dominant.

4.2. Bullet Evolution: Transverse Field Cases

For the transverse cases where the initial field crosses the bullet's path, field lines are also swept and stretched around the bullet. However in this case the field lines do not reconnect around the bullet, except in a "magnetotail" along the axis, so that a region of high magnetic pressure develops on the bullet nose as shown in Fig. 2. Even in the T5 case with $\beta_0 = 256$, the field is strong enough that $\beta \sim 5$ on the bullet nose by $t/t_{bc} = 2$. For all the other transverse field cases we computed, $\beta \lesssim 1$ along the nose of the bullet by this time. In models T1 and T2, $\beta < 10^{-1}$ here and $p_b \sim \rho_a u_b^2$ directly on the leading edge of the bullet. Except in T5, $\beta \lesssim 10^{-1}$ along the top and towards the rear of the bullet boundary, partly because the gas pressure is low, but mostly because field lines have been greatly stretched. That characterization of the field lines is obvious in Fig. 2 or Fig. a2. Even though field lines are compressed by the bow shock, it is stretching, not compression, that is important to the evolution of the magnetic field and to its eventual dynamical role. That supports the expectations expressed by Jones, Kang, & Tregillis 1994, based on passive fields. One can see in Fig. 6 that the normalized magnetic energy enhancement for the transverse geometry grows to more than 10^3 for the weakest field cases and more than 10^2 even for the strongest field cases. Since the volume containing highly compressed plasma is never more than a few times the initial bullet volume, the maximum field enhancement through compression would be $\lesssim 10\ E_{Bob}$, emphasizing the importance of stretching. We note that the magnetic energy in the transverse cases seems fairly well converged through the full duration of the simulations and better than in the aligned field geometry. That makes sense, since the transverse fields are not so closely tied to vortical flows behind the bullet.

We can write down a crude model for the enhancement of the magnetic field energy in the transverse cases that seems to qualitatively account for what is seen. For ideal MHD the magnetic induction equation can be expressed in a form

$$\frac{d \ln B/\rho}{dt} = \frac{B \cdot [(B \cdot \nabla) u]}{B^2}, \tag{8}$$

where $d\ /dt$ is the convective derivative. At the stagnation point on the bullet nose we can estimate $\nabla \cdot u \lesssim \frac{1}{4} u_{b0}/R$ and $B \cdot [(B \cdot \nabla)u] \sim B^2 u_{b0}/R$, so that

$$\frac{d \ln B^2}{d(t/t_{bc})} \sim \alpha \chi^{\frac{1}{2}}, \tag{9}$$

where $\alpha \sim 1$ is a "fudge factor" accounting for various details. If this field growth occurs within a "shield" of volume $V_{shield} \sim R^2$, we can estimate the associated magnetic energy enhancement to be

$$\Delta E_{mag} \sim few \times \exp\left(\alpha \chi^{\frac{1}{2}} \frac{t}{t_{bc}}\right). \tag{10}$$

That growth seems consistent with the results shown in Fig. 6, for $t/t_{bc} \lesssim 2$. Since the field on the bullet nose saturates with $p_b \sim \rho_a u_{b0}^2$, we expect a maximum for $\Delta E_{mag} \sim few \times \beta_0 M^2$. That is also roughly consistent with the results in Fig. 6. The early magnetic energy enhancement is similar for all the values of β_0, but it saturates sooner and the dynamical influence of the field is sooner when β_0 is smaller.

The field lines draped over the bullet are also drawn down near the symmetry axis into the bullet wake, producing a region that resembles the flux rope seen in the aligned field cases. Again, this is a region of $\beta << 1$, but primarily because the gas pressure is very low from the initial evacuation of this region. It is always the case in our simulations that $p_b << \rho_a u_b^2$ within this feature. In addition, the $y = 0$ boundary of our grid separates field lines of opposite direction; *i.e.*, there is a current sheet there, much as in the earth's magnetotail. That is also unstable to tearing mode instabilities that limit fields in this region.

Like the earth's magnetosphere does, the penetration of the bullet through a "quasi-transverse" field should produce on the bullet nose an induced electric field perpendicular to both the magnetic field and the bullet velocity. In this case that projects out of the computational plane. If the third dimension of the bullet $\sim R$, then the induced potential across the bullet would be $\Phi \sim u_{b0} B R/c$. Taking numbers that might be appropriate for knots in a young SNR like Cas A ($B \sim 10^{-4}$ Gauss, $u_{b0} \gtrsim 10^{-3}$ c, $R \sim 10^{16}$ cm) (*e.g.*, Anderson *et al.* 1994), we find that $\Phi \gtrsim 10^{11}$ Volt is possible. Supposing that reconnection within the bullet magnetotail can generate electric fields aligned with the magnetic fields, then these regions might be important sites for nonthermal particle acceleration.

For the weak transverse field cases, the bullet dynamics initially resembles the aligned field and gasdynamical cases to the first approximation. The R-T bubbles seen in those other situations form here, too. In fact at $t/t_{bc} = 2$ there are no obvious differences in either bullet morphology or flow dynamics between models A5 and T5, for example (see Figs. 1 and 3). As time progresses, however, the bullet in all transverse field cases becomes significantly influenced by the field. Even though the same "C"-shaped bullet morphology is seen in the two weakest field cases, T4 and T5, field stretched over the top and back of the "C"-shaped cloud develops magnetic pressures significantly greater than the gas pressure, so that $\beta < 1$ along the bullet edge. This condition protects the bullet from further disruption. In model T5 that happens quite late, so as late as

$t/t_{bc} = 6$ the bullet morphology is pretty similar to A5. However, even in model T4 ($\beta_0 = 64$) the field becomes dynamically strong ($\beta \sim 1$ along the bullet nose just after $t/t_{bc} = 2$). That case still expands laterally, but not so fast as in the cases with negligible magnetic influence (see Fig. 6). For all the other transverse cases with $\beta_0 \leq 16$, the Maxwell stresses grow large enough to completely inhibit lateral expansion of the bullet. The bullets are then enshrouded by a strong magnetic shield. For cases involving an initially weak field, the bullet is partially disrupted, but eventually the shield protects the R-T fingers from further erosion. The bullet embedded in a stronger field is compressed, but then, as the field confines it, develops a streamlined profile and is not strongly eroded.

Remarkably, Fig. 6 shows that the acceleration of the transverse-field bullet increases with the strength of the magnetic field. This trend is reversed from that of aligned-field bullets. There we have observed that the tendency of stronger field to resist lateral expansion reduces the evolution to a greater cross section. It was that increased cross section and the augmented drag that were modified by the field. For the transverse field models, lateral expansion can be halted entirely, yet the drag force clearly is enhanced with the stronger field. This seeming paradox is easily explained by accounting properly for the role of the magnetic pressure in the drag. Whereas the aligned field did not contribute directly to the force across the bullet, the transverse field does. The MHD Bernoulli equation on the symmetry axis gives the result in the highly supersonic limit that $\Delta p = \Delta(p_g + p_b) \approx (4/5)\rho_a(u_x - u_{b0})^2 + (1/5)p_b$, where $p_b = \frac{1}{2}B_y^2$ on the nose of the bullet in this case. As already noted, p_b increases over the first few crushing times and can become comparable to $\rho_a u_b^2$ in that region. Although the expansion coefficient $C_e = 0$ in Eqs. 6 and 7 the drag coefficient, C_d, is an effectively increasing function of time and that enhances the bullet's acceleration. We find, for example, that Eq. 7 gives a good fit to the motion of the strongest field case, T1, by setting $C_e = 0$, replacing C_d with $C_d(1 + 0.01t/t_{bc})$, and using the same $C_d = 1.0$ that we have used for aligned field models. That corresponds to an increase in drag of about 5% at the end of the simulation.

Thus, the picture that develops for the transverse field bullets is rather different from and considerably simpler than the ones for aligned field. Magnetic field is swept around the bullet to form a protective shield. The magnetic pressure becomes comparable to the ram pressure through the bullet bow shock; thus, the magnetic energy is enhanced by an amount approaching $\sim M^2\beta_0 p_{b0} V_{shield}$. Again taking that to be roughly the volume of the bullet, we recover the observed magnetic energy enhancements with the expression $\Delta E_{mag} \sim \beta_0 M^2$. Our bullets have a cylindrical form, so that field lines cannot be swept around the sides of the bullet in the z-direction. Such sweeping may reduce the magnetic field enhancement somewhat in a three-dimensional bullet. But we still expect the same qualitative behavior, since much of the field that forms into the shield comes from the field lines that penetrate into the "skin" of the bullet, and since irregularities in the spherical bullet would capture field lines much like the cylindrical one does.

The brief summary of transverse bullet evolution is the following. Even when the initial field is of modest strength measured in terms of the ratio of magnetic pressure to background plasma

pressure, the stretched magnetic field effectively confines the bullet and prevents its fragmentation. Further, the magnetic pressure applied to the nose of the bullet increases the rate at which the bullet is brought to rest with respect to the ambient medium; more effectively, in fact, than the lateral expansion that accompanies the acceleration of gasdynamical bullets.

5. Summary and Conclusions

We have carried out an extensive set of two-dimensional MHD simulations exploring the role of magnetic field in the dynamics of supersonic clumps of plasma. We have examined the influence of both field strength and orientation on the problem. Of those two characteristics field orientation is far more important. Even a very modest ambient magnetic field that crosses the path of the bullet tends to be amplified by field line stretching around the bullet until the Maxwell stresses become comparable to the ram pressure associated with the bullet motion. A field that is aligned with the bullet motion, on the other hand, develops reconnection-prone topologies that shorten the stretched field and release the excess energy it contains. The field is also swept around the bullet in this geometry and can temporarily become moderately strong. However, the energy in the field is not enhanced so much for this geometry as for the transverse geometry. Rather, as a consequence of reconnection, there is a transformation and relaxation of the field over a few bullet crushing times. Some magnetic flux passes directly through the bullet, where it can become entrained in vortices and amplified around the vortex perimeter. The remaining flux passes directly around the bullet, where it can act to resist lateral expansion as it is stretched by that expansion. In this geometry, however, the Maxwell stresses on the bullet never approach the ram pressure level. Even so, a field of even moderate initial strength becomes strong enough to help realign the flow around the bullet into a smoother, more laminar form that reduces the tendency of the bullet to fragment.

Both of the above field geometries are highly idealized, and more generally the bullet would encounter a field at some oblique angle to its motion. In that situation, we will want to know which of the two special cases is more relevant. The most important detail should be if, as the field lines are swept over the bullet, they are folded over the top as well, thus leading to reconnection. Conceptually that depends on the relative rates at which the field lines are swept past the bullet body, on the one hand, and at which the "foot-points" of the field lines along the bow shock move past the bullet, on the other hand. If the field-line bow-shock foot-point moves faster (as it must for transverse field cases), the lines are not folded over the top, but stretched directly to the bow shock. If, however, the field-line bow-shock foot-point moves slower (it is at rest for aligned field cases), then the field lines are folded over inside the bow shock on one side of the bullet and likely to reconnect. We can derive an approximate expression for the condition that the field foot-point moves downstream faster than the flow around the bullet, if we take the Mach bow shock to be a simple cone with half angle $\arctan(1/\sqrt{M^2-1})$ and suppose that the flow speed around the bullet is $u = \delta u_{b_0}$. Defining the motion of the foot-point as the translation of the intersection between

the field line and the bow shock, this leads to the constraint

$$\tan\theta \gtrsim \frac{\delta}{(1\ -\ \delta)\sqrt{M^2-1}}, \tag{11}$$

where θ is the angle between the bullet motion and the ambient magnetic field. In the limit $M >> 1$, with $\delta \sim 1/2$, this becomes

$$\tan\theta \gtrsim \frac{1}{M}. \tag{12}$$

So, we conclude that for supersonic bullets most field directions will lead to behaviors similar to the transverse field cases, while as the motion becomes transsonic the dividing line would be closer to 45°. Except in circumstances with preferential alignments between the motion and the field, that would lead to the further conclusion that even a weak magnetic field will have a substantial impact on the evolution and dynamics of supersonic clumps of ionized, conducting gas. In young supernova remnants, polarized radio synchrotron emission indicates that there is a net radial direction to the magnetic field inside the remnants (Milne 1987). This might suggest that bullets in young remnants would generally encounter a radial field and, hence, one nearly aligned with their motions. That view is somewhat simplistic, however, because the same radio observations also show a very small net polarization (Anderson, Keohane, & Rudnick 1995) indicating that, to first order, the field is disordered. That, in turn, argues that a wide range of field orientations may be encountered by small projectiles.

In either limiting field geometry and presumably those in between, field line stretching is the dominant process for magnetic field amplification. That supports the conclusions reached by Jones & Kang 1993 and Jones, Kang, & Tregillis 1994 that nonthermal radio emission associated with supersonic clumps in supernova remnants, for example, is likely to be largely controlled by the generation of stretched magnetic fields around the perimeters of the clumps, rather than primarily highlighting the bow shock where field is mostly enhanced by compression. We note that the structures of the bow shock and the bullet boundary may even superficially resemble each other in observations, so that morphology alone can be misleading. The physical difference is important, however, since the bow shock is probably the site of local particle acceleration, while on the bullet perimeter one sees primarily energetic particles that come from some other site (possibly including the bow shock, of course). Our estimates of the field strengths expected in the two situations are very different, however. So, observational estimates of the local magnetic field (based on equipartition, for example) would possibly lead us to very different conclusions about the local conditions.

In addition, since the magnetic pressure on the nose of the bullet may become comparable to the ram pressure and hence the total pressure behind the bow shock, the gas pressure there could be substantially lower than that in a gasdynamical bullet. That means, as well, that the temperature in the region on the nose of the bullet would be lower than that predicted in the gasdynamical case. That detail can alter expectations of the thermal emission, including X-rays and UV-IR lines.

In summary, the role of a magnetic field in the evolution and in the appearance of supersonic clumps is very important, even if the magnetic field is nominally not strong in the ambient medium. The importance comes because magnetic field lines can be stretched and amplified if they become draped around the bullet perimeter. That effect seems especially strong when the field lines are "quasi-transverse" to the motion, a concept that depends on the speed of the bullet, but seems to include most directions. Additional amplification within vortices associated with the destruction of the bullets can also occur, but seems to be less important. If the fields are quasi-transverse, then they can effectively confine the bullet and prevent its disruption. The same amplified fields may be important to emissions used to analyze the bullets. They can control the radio synchrotron emission expected and possibly become strong enough to alter the local thermodynamics of the gas and influence thermal emissions, as well.

We are grateful to Adam Frank, Byung-Il Jun, Bob Lysak and Larry Rudnick for fruitful discussions and to Mordecai-Mark Mac Low for helpful comments on the manuscript. At the University of Minnesota this work was supported in part by NSF (AST-9318959), NASA (NAGW-2548), and the Minnesota Supercomputer Institute. At Chungnam National University this work was supported in part by the Basic Science Research Institute Program, Korean Ministry of Education 1995, Project No. BSRI-95-5408.

A. Numerical Grid Issues

We have carried out several experiments to understand the influence of finite numerical resolution on our simulations. There are two issues. First, we are nominally simulating ideal MHD, but depend on the existence of a small, albeit finite, dissipation on the grid cell scale to simulate the physical viscous and resistive dissipation that certainly takes place on very small scales. The existence of the numerical dissipation is necessary, for example, to allow shocks to form and magnetic reconnection to occur. There is fairly good evidence that conservative monotonic schemes such as ours do a good job of approximately representing physical viscous and resistive dissipative processes presumed to exist on scales somewhat smaller than the grid (*e.g.*, Porter & Woodward 1994). For the astrophysical environments being simulated, the dissipative scales are probably very much smaller than those that can be modeled directly, however. Thus, the numerical solutions, if they are complex, will generally differ to some degree from the asymptotic "physical" solution on the smallest scales after long periods of time. One hopes, on larger scales and over moderate periods of time, that the behaviors will be converged for important characteristics. Our code is second-order accurate in smooth flows, so that the effective Reynolds numbers increase with length, l, approximately as $R_e \sim K(l/\Delta x)^2$ where Δx is the size of a computational zone (Ryu, Jones, & Frank 1995). For moderately strong magnetic fields ($\beta \sim 2$), $K \approx 0.5$ in our code. For much weaker fields the dissipation is several times less on a given scale. In any case, we expect that dissipation would be confined to scales of only a few zones and that *inertial* structures

formed within scales of less than $10 - 20$ zones would have histories that are resolution-dependent. The second, related issue has to do with the fact that the late history of a bullet depends on the nonlinear evolution of instabilities that in our simulations form off of the initial surface of the bullet. Consequently that history can depend to some degree on the exact structure of the initial perturbation in a way that extends beyond the size scale of the perturbation.

Most of our simulations (T1–T5 and A1–A5) have been conducted using a grid placing 50 zones across the bullet radius (R_{50}) and with the bullet centered in the middle of a zone along the bottom axis ($y = 0$). To evaluate the importance of the zone size on our calculations, we have carried out simulations identical to T5 and A5 except that 100 zones spanned the bullet radius (R_{100}; T6 and A6). In addition, we have performed a number of test runs with varying resolution using this code but setting the magnetic field strength to zero. In some of those, we have simulated the impact of a Mach 10 shock on the cloud. The intent there was to repeat the resolution tests shown in Mac Low *et al.* 1994. Since they used cylindrical geometry, and we have used Cartesian geometry, an exact comparison is not meaningful. But we conclude that our MHD code produces resolution dependencies very comparable to those they displayed as computed from their gasdynamical code.

Some simple illustrations make plain the limitations imposed by our grid. Fig. a1 compares the density structures computed for models T5 and T6 (top panels) as well as A5 and A6 (bottom panels). Results in each case are shown at two times, $t/t_{bc} = 4/3$ and 4, with the earlier time displayed above the later time. Fig. a2 displays the magnetic field structures for the same cases. R_{50} runs, T5 and A5, are shown on the left and R_{100} runs, T6 and A6, on the right. These have the weakest initial fields of any of the simulations we have run in this study. They are, thus, the cases where we would expect the greatest dependence on numerical resolution, since a strong magnetic field has a tendency to produce smoother flows and more organized field structures. At $t/t_{bc} = 4/3$ the paired runs agree almost exactly for both field configurations. At $t/t_{bc} = 4$ the structural agreement is qualitatively consistent, but there are clear differences. Especially in the magnetic field lines shown in Fig. a2, there is additional fine structure in the higher resolution runs. Also the field along the leading edge of the bullet is somewhat stronger in the higher resolution runs. Both of these features are anticipated, since they come directly from the reduced dissipation scale in the R_{100} runs. Most apparent, however, is that the instabilities that begin to destroy the bullet have a somewhat different nonlinear development; *i.e.*, the shapes of the bullets are beginning to differ.

As it turns out, that result comes at least as much from the fact that the form of the initial perturbations on the bullet is slightly different as a consequence of the different resolutions as from the differences in dissipation scales. The reason is because our initial perturbation results from the mismatch between a circular cross section and a Cartesian grid. Thus, either a change in the number of zones spanning the bullet or a shift in the bullet center will alter the locations of those irregularities. To make that point clear, we compare in Fig. a3 the density distributions for two R_{50} runs at $t/t_{bc} = 3$ and 5. The one shown on the left is A5, while the one on the right is

identical to A5 *except for one small detail*; namely, that the initial bullet center is shifted 1/2 zone to the right from a zone center to a zone edge along the bottom grid boundary. The differences between these two runs are almost as great as those between the two different resolutions, and, in particular, the degree of the changes in bullet shape is comparable. This emphasizes that, once the instability becomes nonlinear, the precise structure becomes sensitive to exact details of the initial conditions.

Considering these comparisons, one should concentrate on more global characteristics than on specific structural features in simulations like those in this paper. In that global sense, the model comparisons are much closer. To demonstrate this, Fig. a4 compares the evolution of the bullet mass, speed, and height as well as the normalized magnetic energy enhancement in the computational domain for each resolution pair (T5,T6 and A5,A6). In each pairing, these important dynamical quantities agree very well. For example, the magnetic energy enhancement in the two transverse field runs approaches $\sim 10^3$ by $t/t_{bc} = 4$. The two runs agree within about 10% on that figure. In the aligned field pair, the enhancement is much smaller and ΔE_{mag} peaks between 50 and 60 for the two resolutions with about 20% more enhancement in the R_{100} run. Those differences reflect, on the one hand, that for the transverse field cases the magnetic field is more effectively stretched, but, on the other hand, that for the aligned field cases the field interacts much more with vortices. Vortex structure and magnetic field behavior there are fairly sensitive to numerical resolution. Overall, it is clear that run pairs are largely consistent with each other. Slightly less stripped bullet material has left the grid in each of the high resolution runs at the last time shown, but is less than 1% of the bullet mass, in any case.

Table 1. Summary of Simulations Reported

Model[a,b]	Resolution[c]	β_0[d]	M_A[d]	χ	t_{bc}[e]	t_{end}
T1 (A1)	R_{50}	1	9.13	10	0.6	5 t_{bc}
T2 (A2)	R_{50}	4	18.3	10	0.6	8 t_{bc}
T3 (A3)	R_{50}	16	36.5	10	0.6	8 t_{bc}
T4 (A4)	R_{50}	64	73.0	10	0.6	8 t_{bc}
T5 (A5)	R_{50}	256	146	10	0.6	8 t_{bc}
T6 (A6)	R_{100}	256	146	10	0.6	4 t_{bc}
N1	R_{50}	∞	∞	10	0.6	2 t_{bc}
N2	R_{50}	∞	∞	40	1.2	2 t_{bc}
N3	R_{50}	∞	∞	100	2.0	2 t_{bc}

[a]All models have used $\gamma = 5/3$, $M = 10$, $u_{b0} = 10$, and $c_{sa} = 1$.

[b]Models with fields transverse to the bullet motion are designated by the letter "T", fields aligned with the motion by the letter "A" and those with no magnetic field by the letter "N". All the "T" and "A" models have been done in pairs, with otherwise identical characteristics.

[c]Code indicates the number of computational zones spanning the initial bullet radius. That radius corresponds to 0.97656 in the full computational domain which has dimensions $x \times y = 10 \times 5$.

[d]$\beta_0 = p_g/p_b = (2/\gamma)(M_A/M)^2$, defined in terms of background plasma values.

[e]Values of the bullet crushing time used in the discussion. For $\chi = 10$ and 40 these times have been rounded down slightly for ease of matching to simulation dump times.

REFERENCES

Allen, D. A., & Burton, M. G., 1993, Nature, 363, 54.

Anderson, M. C., Jones, T. W., Rudnick, L., Tregillis, I. L., & Kang, H., 1994, ApJ, 421, L31.

Anderson, M. C., Keohane, J. W., & Rudnick, L., 1995, ApJ, 441, 300.

Aschenbach, B., Egger, R., & Trümper, J., 1995, Nature, 373, 587.

Brackbill, J. U., & Barnes, D. C., 1980, J. Comput. Phys., 1980, 75, 400.

Braun, R., Gull, S. F., & Perley, R. A., 1987, Nature, 327, 395.

Cattaneo, F., & Vainstein, S. I. 1991, ApJ, 376, L21.

Chandrasekhar, S., 1961, Hydrodynamic and Magnetohydrodynamic Stability (new York: Oxford Univ. Press).

Coleman, C. S., & Bicknell, G. V., 1985, MNRAS, 214, 337.

Frank, A., Jones, T. W., Ryu, D., & Gaalaas, J., 1996, ApJ, (April 1, 1996, in press).

Galloway, D. J., & Weiss, N. O., 1981, ApJ, 243, 945.

Jones, T. W., & Kang, H., 1993, ApJ, 402, 560.

Jones, T. W., Kang, H., & Tregillis, I. L., 1994, ApJ, 432, 194.

Klein, R. I., McKee, C. F., & Colella, P. 1994, ApJ, 420, 213.

Loeb, A., Rasio, F. A., & Shaham, J., 1995, Preprint

Mac Low, M., McKee, C. F., Klein, R. I., Stone, J. M., & Norman, M. L., 1994, ApJ, 433, 757.

Mac Low, M. & Zahnle, K. 1994, ApJ, 434, L33

Milne, D. K., 1987, Austr. J. Phys, 40, 771.

Norman, C., & Silk, J., 1979, ApJ, 228, 1979.

Porter, D. H., & Woodward, P. R., 1994 ApJS, 93, 309.

Ryu, D., & Jones, T. W., 1995, ApJ, 442, 228.

Ryu, D., Jones, T. W., & Frank, A., 1995, ApJ, 452, 785.

Schiano, A. V. R., Christiansen, W. A., & Knerr, J. M., 1995, ApJ, 439, 237.

Stone J. M., Xu, J., & Mundy, L. G., 1995, Nature, 377, 315.

Schwartz, R. D., 1975, ApJ, 195, 631.

Strom, R., Johnston, H. M., Verbunt F., & Aschenbach, B., 1995, Nature, 373, 590.

van den Bergh, S., 1971, ApJ, 165, 457.

Weiss, N. O., 1966, Proc. Roy. Soc. London, A., 293, 310.

Xu, J., & Stone, J. M., 1995, ApJ, 454, 172.

Zahnle, K. J. 1992, J. Geophys. Res.(E), 97, 10243

FIGURE CAPTIONS

Fig. 1 Grayscale images of the log density for models T2 (a), T5 (b), A2 (c), and A5 (d) at two times ($t/t_{bc} = 2,\ 6$) (top and bottom, respectively). This shows bullet evolution for strong and weak magnetic fields ($\beta_0 = 4,\ 256$) and for both transverse and aligned magnetic field geometries. Values increase from dark tones to high tones.

Fig. 2 Same as Fig. 1, except showing the magnetic field lines (contours of the magnetic flux function). About 40 equal-interval contours of flux function are shown in each frame.

Fig. 3 Same as Fig. 1, except showing the grayscale images of the vorticity. Dark tones are negative vorticity while high tones are positive.

Fig. 4 Grayscale images of the log density for gasdynamical bullets ($\beta_0 = \infty$). The three runs shown have $\chi = 10$, (a); $\chi = 40$, (b); and $\chi = 100$, (c). Otherwise, the simulations are identical to MHD R_{50} simulations. Each model is shown at $t/t_{bc} = 1$ (top) and $t/t_{bc} = 2$ (bottom).

Fig. 5 Cuts along $y = 0.05$ (or the third cell from the bottom axis with $y = 0$) for models T2 (a), T5 (b), A2 (c), and A5 (d) at the same time as in Fig. 1. Solid lines correspond to $t/t_{bc} = 2$, while dotted lines represent profiles at $t/t_{bc} = 6$. Shown top to bottom are: log gas density, ρ, velocity as measured in the initial rest frame of the bullet, u_x, log gas pressure, p_g, and log magnetic pressure, p_b. nd log magnetic energy enhancement, ΔE_{mag} (Eq. 5).

Fig. 6 Evolution of various integrated quantities. Panel (a) presents values for models with transverse magnetic fields (T1–T5), while panel (b) for models with aligned fields (A1–A5). The line types distinguish models of different initial field strength: solid ($\beta_0 = 1$), long dash ($\beta_0 = 4$), short dash ($\beta_0 = 16$), dot-dash ($\beta_0 = 64$), and dot ($\beta_0 = 256$), with $\beta_0 = p_g/p_b$. Shown top to bottom are: total bullet mass inside the grid, M_{bul} (Eq. 2), mass-weighted bullet speed as measured in the initial rest frame of the bullet, $\bar{u}_b$ (Eq. 3), mean height of the bullet material, $\bar{h}_{bul}$ (Eq. 4), and log magnetic energy enhancement, ΔE_{mag} (Eq. 5).

Fig. a1 Grayscale images of the log density comparing R_{50} with R_{100} runs for both magnetic field geometries when $\beta_0 = 256$. Models T5 (a), T6 (b), A5 (c) and A6 (d) are shown at $t/t_{bc} = 4/3$ and 4.

Fig. a2 Magnetic field lines for the same situations as Fig. a1. About 40 lines are shown in each frame.

Fig. a3 Grayscale images of the log density showing sensitivity of bullet evolution to the initial details along the symmetry axis ($y = 0$). Panel (a) shows model A5 and panel (b) an identical simulation with the initial bullet center shifted along the x-axis 1/2 zone. Times shown are $t/t_{bc} = 3$ (top) and $t/t_{bc} = 5$ (bottom).

Fig. a4 Same quantities as Fig. 6, except now comparing models with different resolution, T5 (dotted lines) and T6 (solid lines) in (a) and A5 (dotted lines) and A6 (solid lines) in (b).

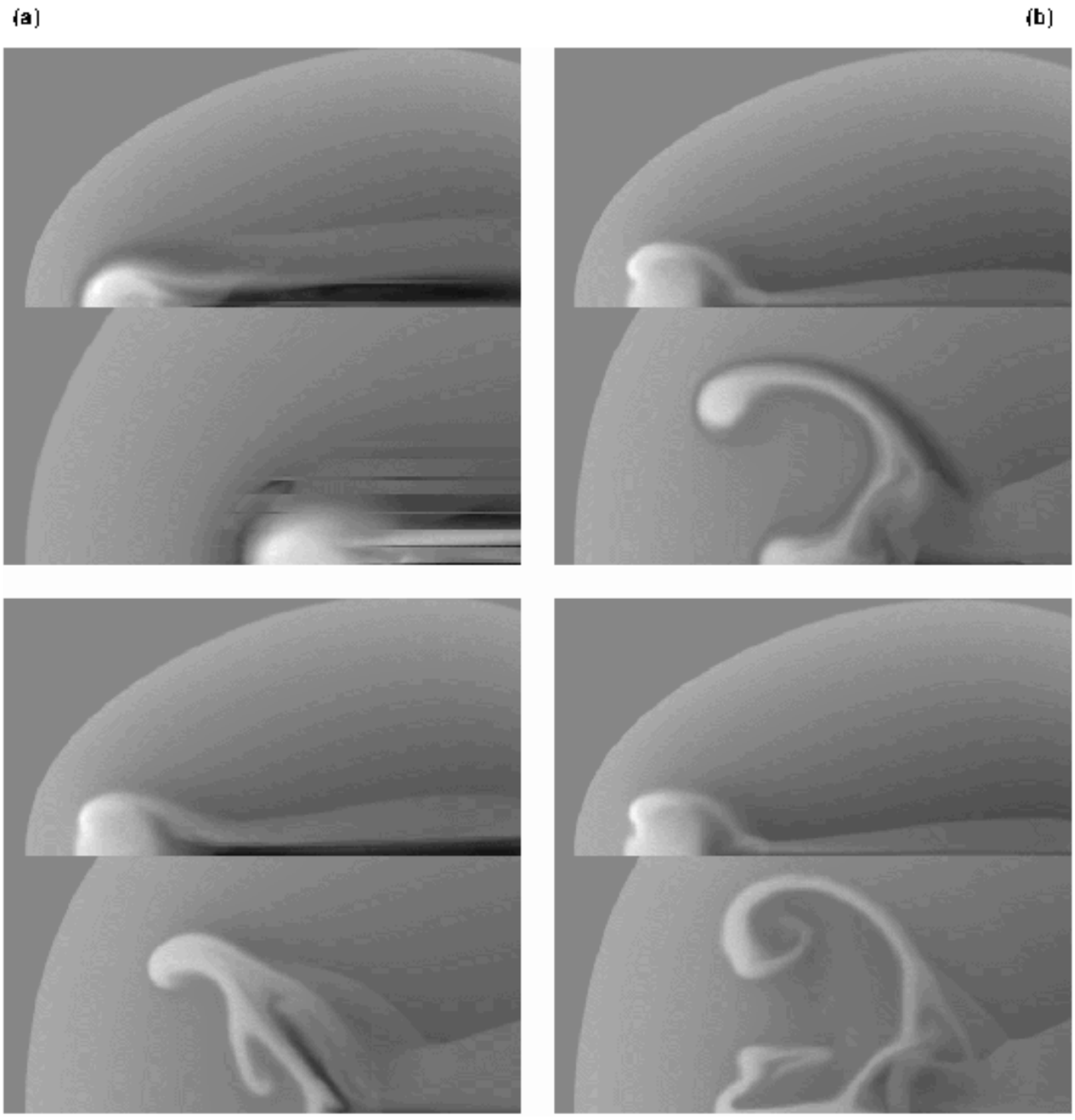

Figure 1

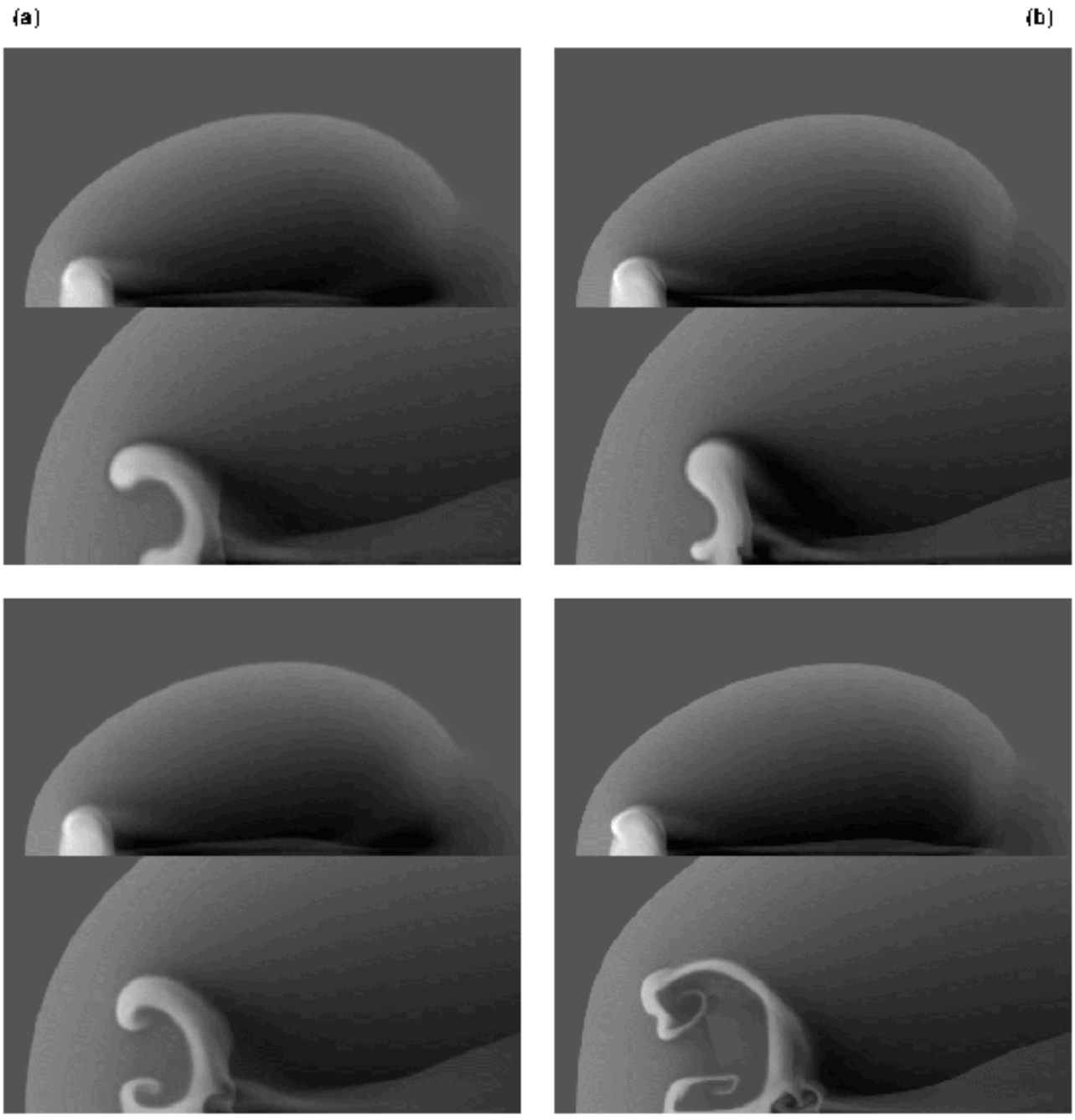

Figure a1

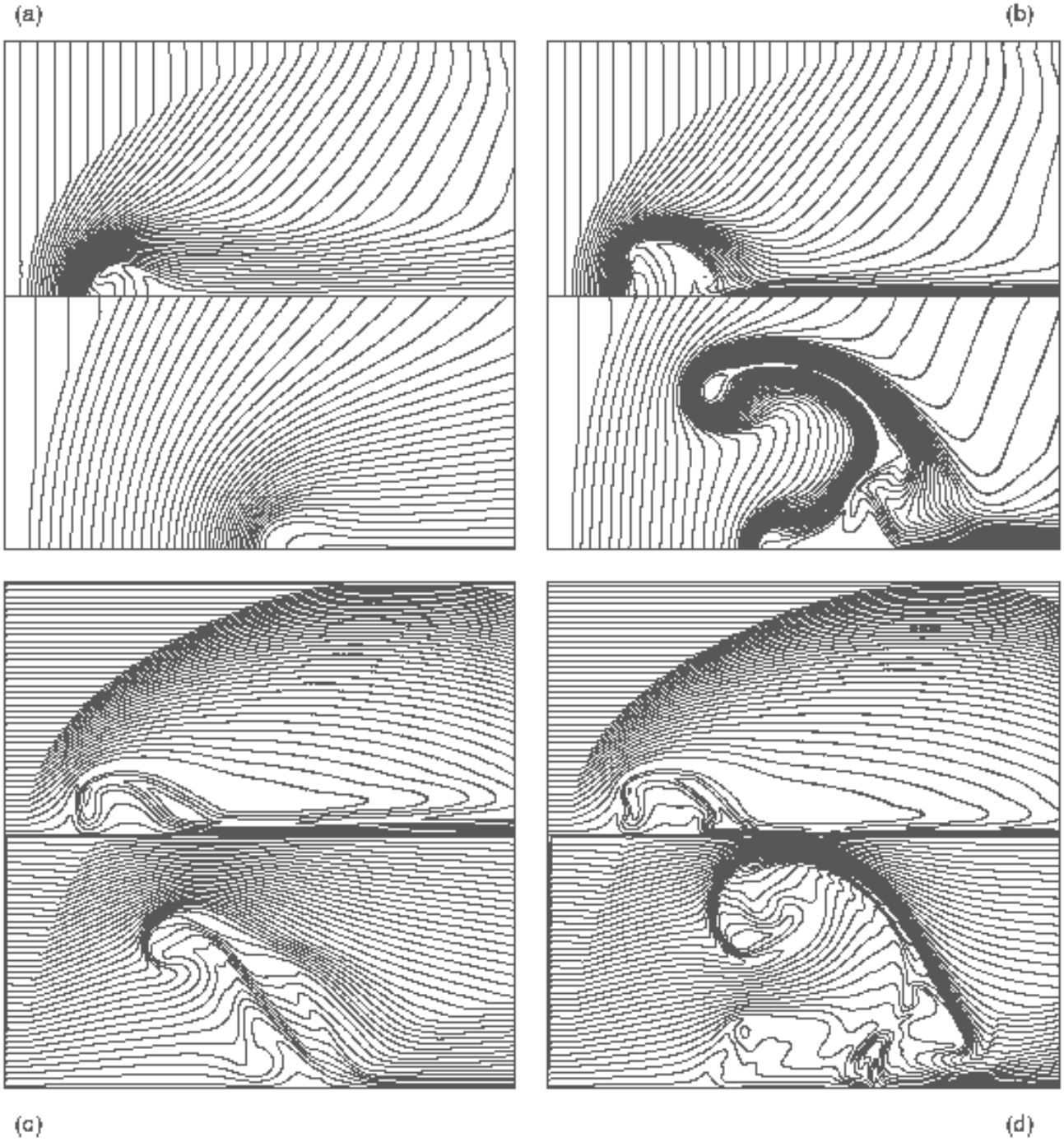

Figure 2

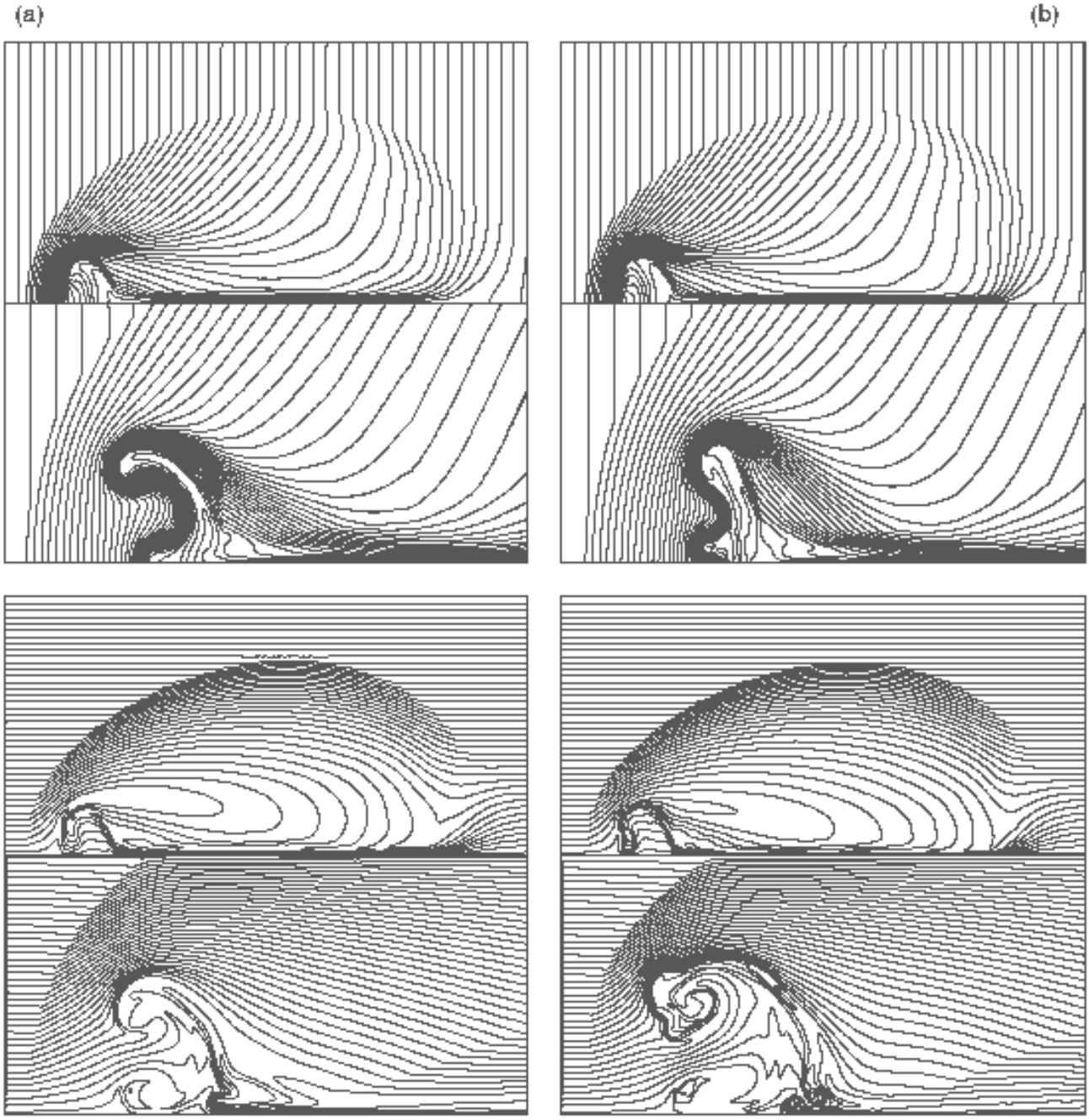

Figure a2

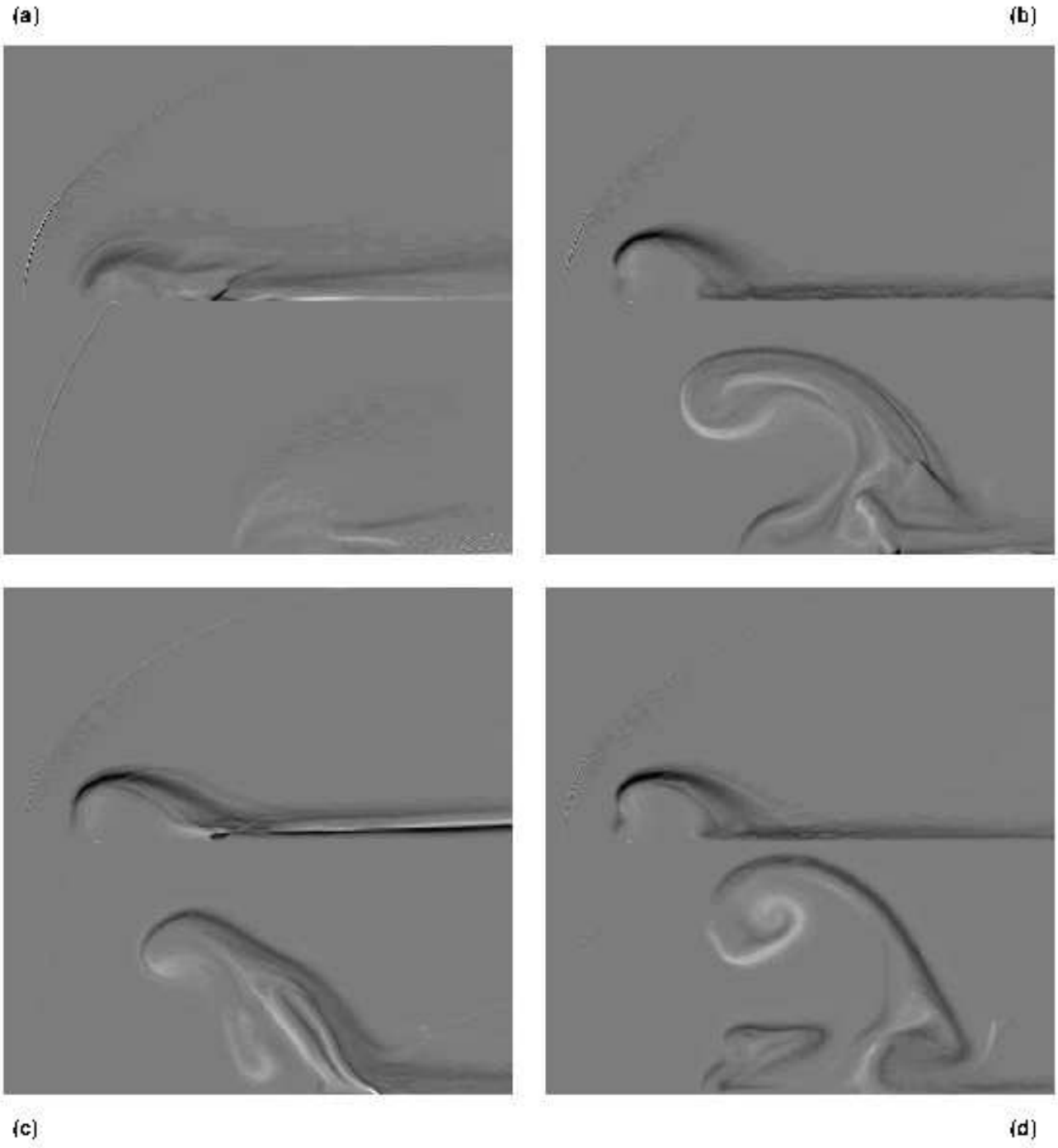

Figure 3

(a) (b)

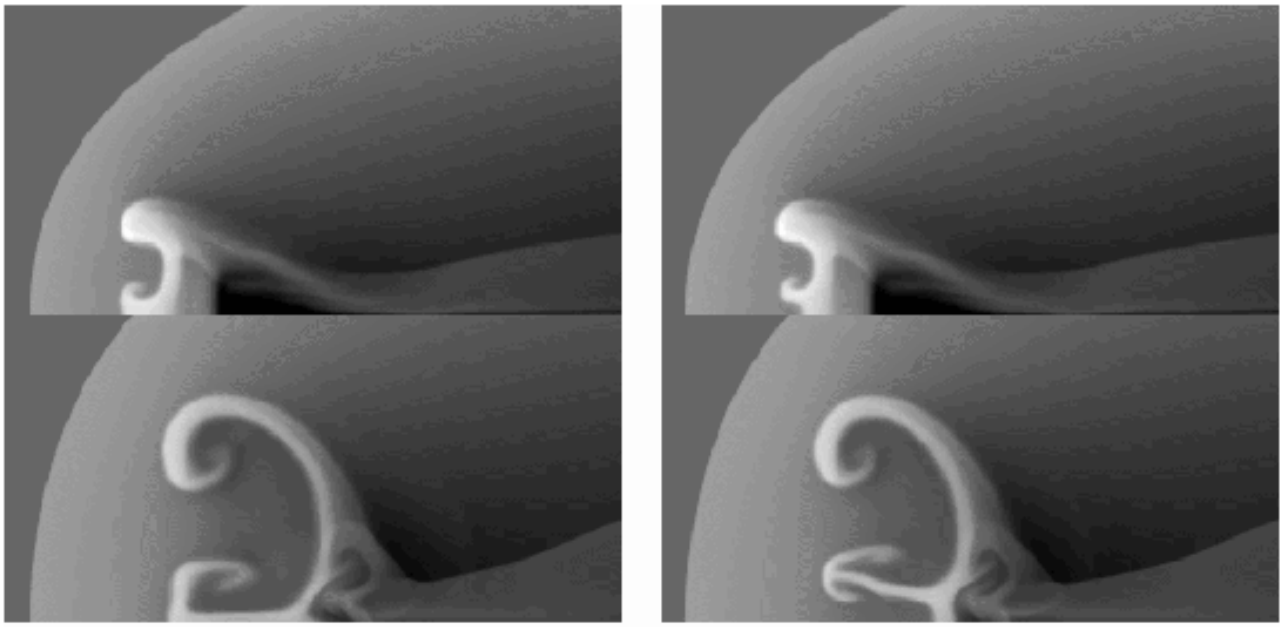

Figure a3

(a)

(b)

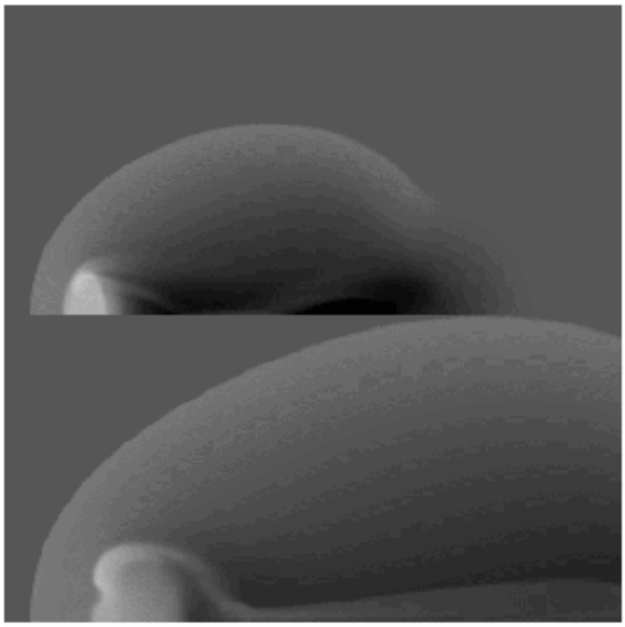

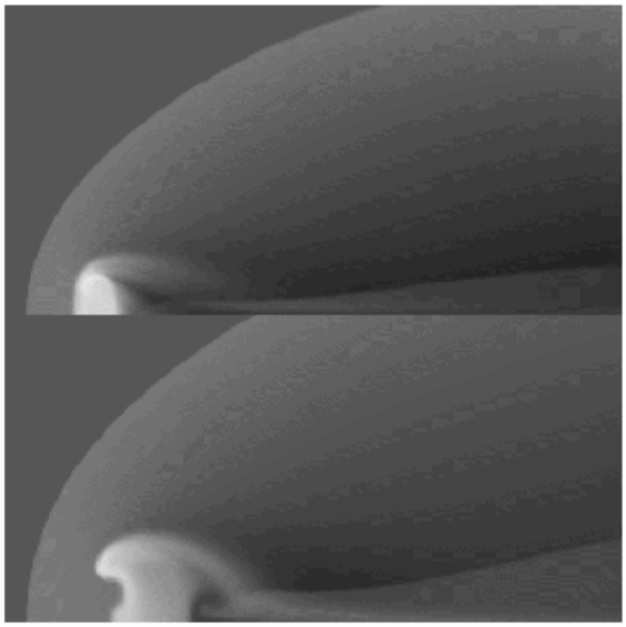

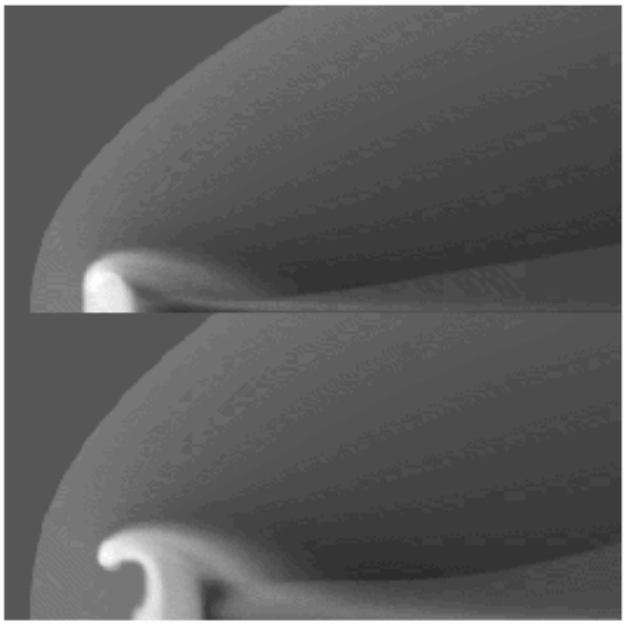

(c)

Figure 4

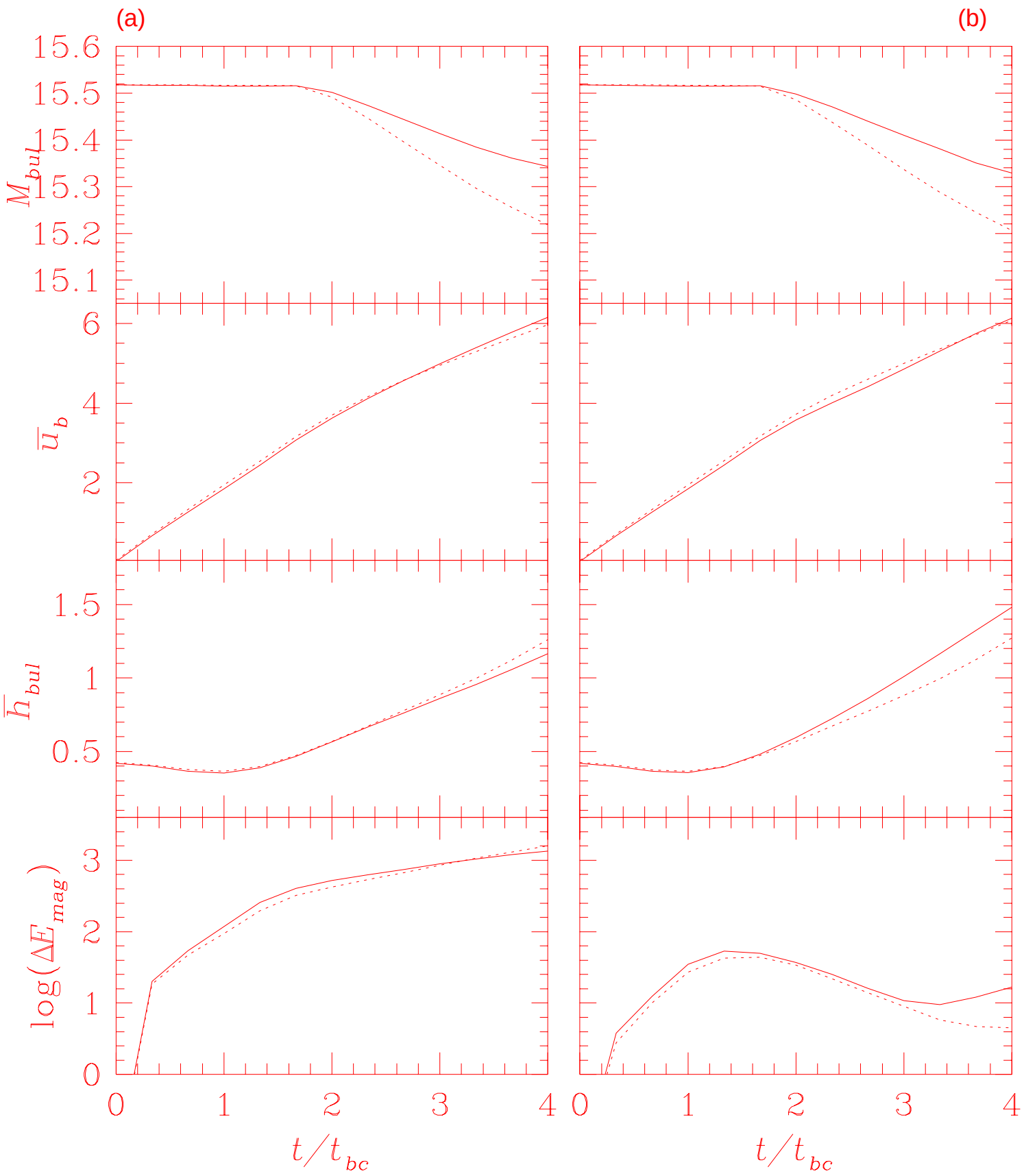
(a)
(b)
15.6
15.5
15.4
15.3
15.2
15.1
M_{bul}
6
4
2
$\overline{u}_b$
1.5
1
0.5
$\overline{h}_{bul}$
3
2
1
0
$\log(\Delta E_{mag})$
0
1
2
3
4
t/t_{bc}

Figure a4

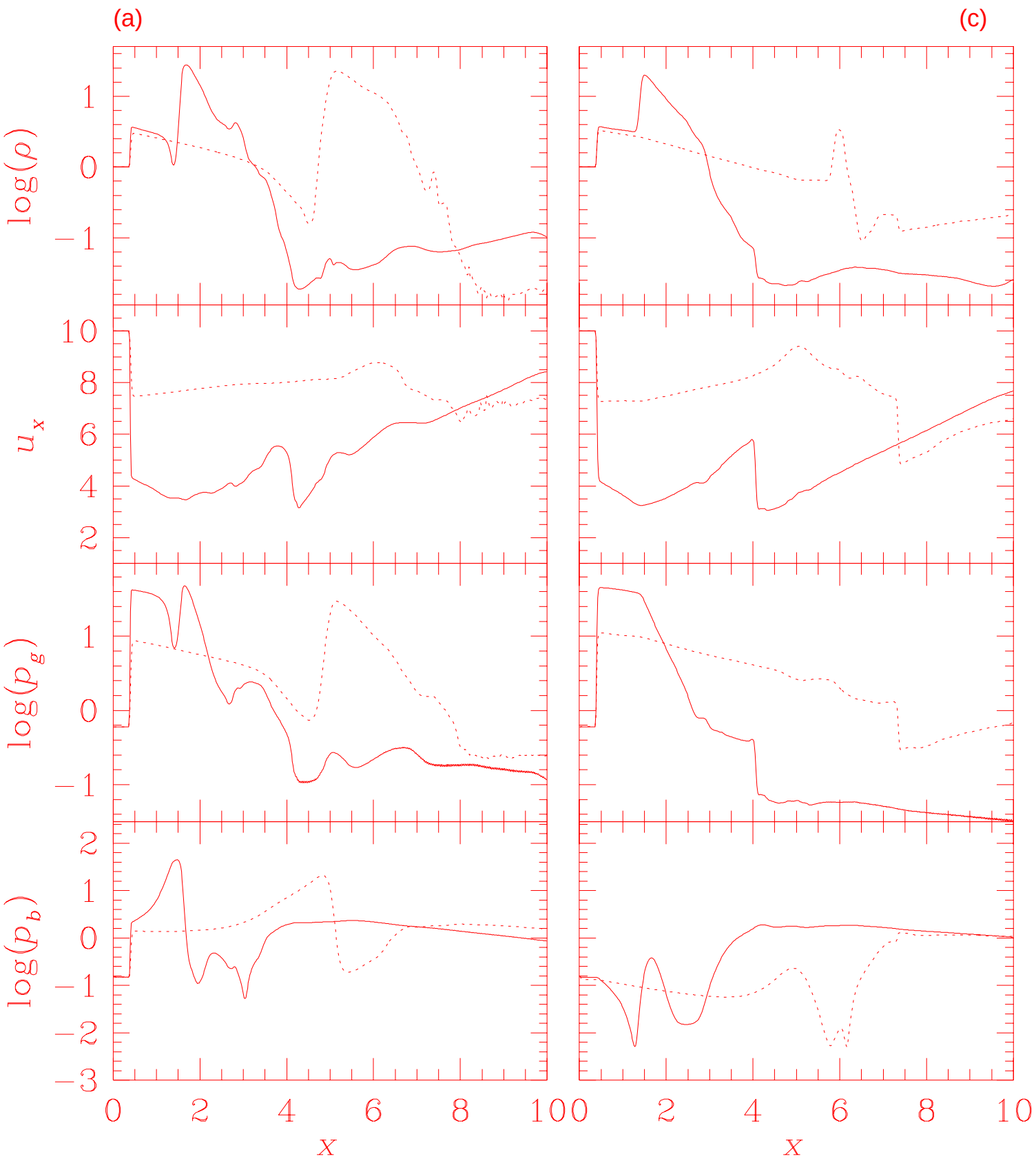

Figure 5

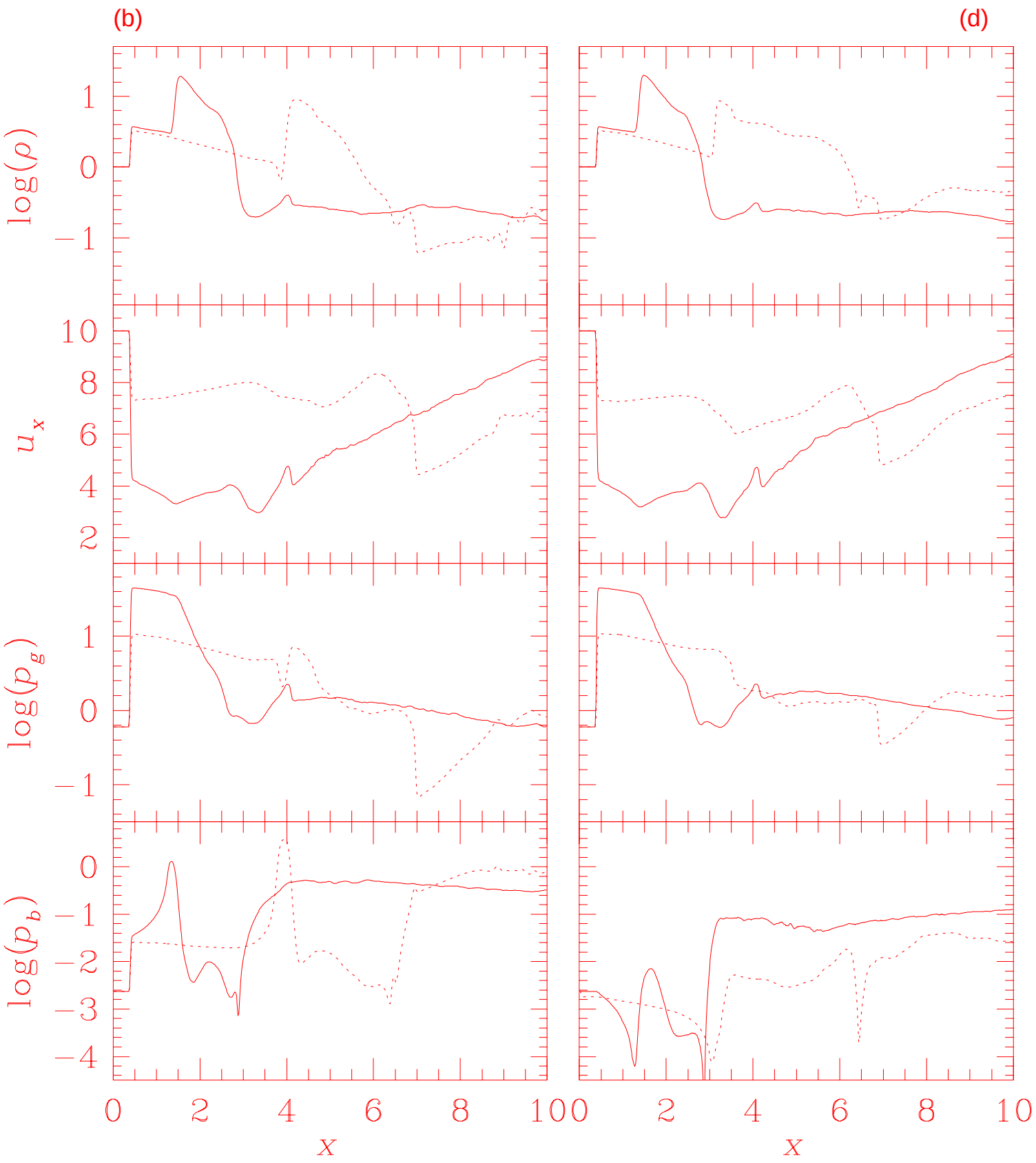

Figure 5

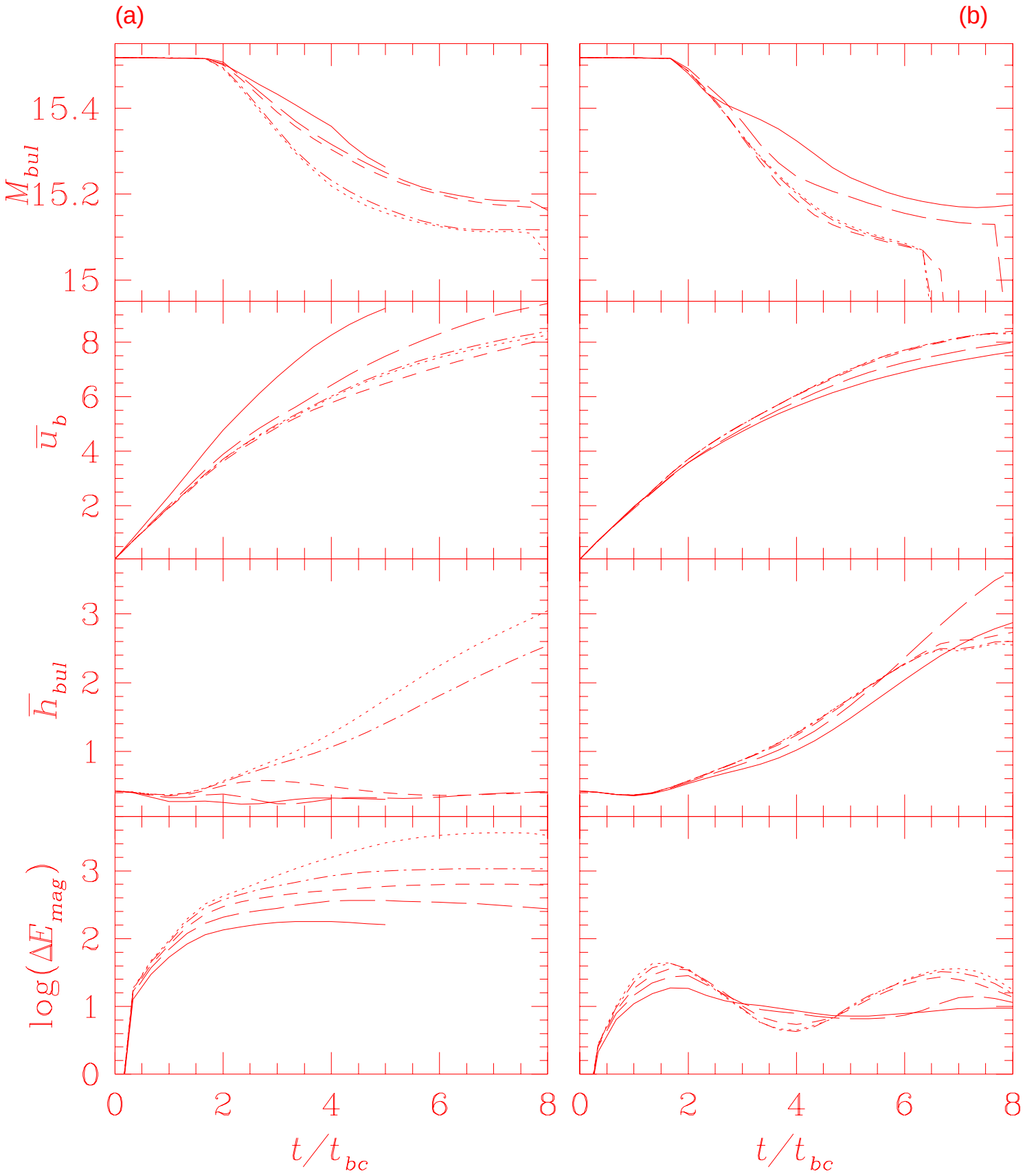
(a)
(b)
M_{bul}
15.4
15.2
15
$\overline{u}_b$
8
6
4
2
$\overline{h}_{bul}$
3
2
1
$\log(\Delta E_{mag})$
3
2
1
0
0
2
4
6
8
t/t_{bc}
t/t_{bc}

Figure 6